Cell Reports

miR-17∼92 exerts stage-specific effects in adult V-SVZ neural stem cell lineages

Graphical abstract

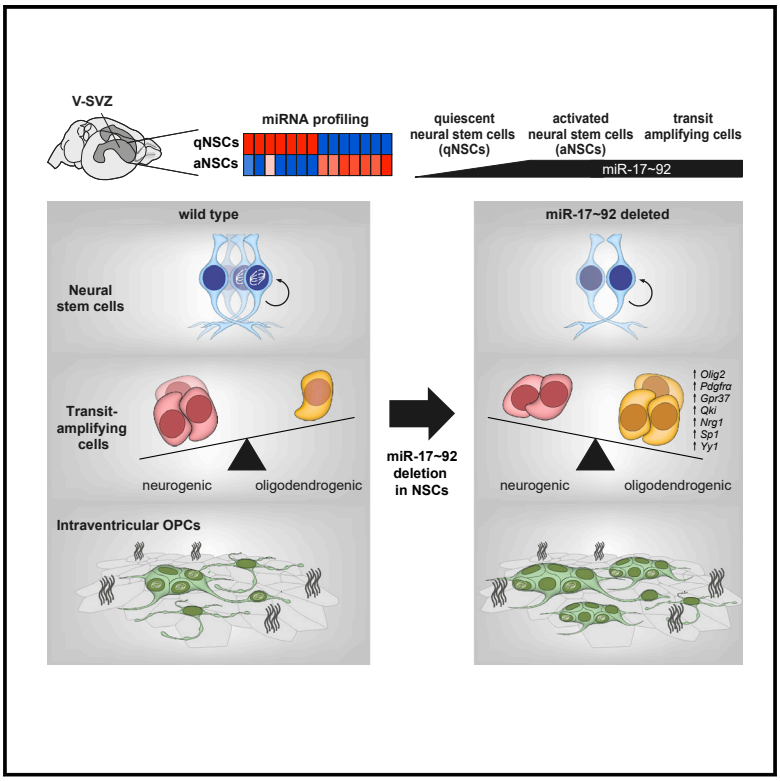

Authors

Fabrizio Favaloro, Annina M. DeLeo, Ana C. Delgado, Fiona Doetsch

Correspondence

fiona.doetsch@unibas.ch

In brief

Favaloro et al. show that adult ventricular-subventricular zone (V-SVZ) quiescent and activated neural stem cells exhibit different microRNA profiles. Using *in vitro* and *in vivo* approaches, they demonstrate that miR-17∼92 regulates neural stem cell proliferation, modulates transit amplifying cell heterogeneity by repressing an oligodendrogenic program, and affects intraventricular oligodendrocyte progenitors.

Highlights

- Quiescent and activated adult neural stem cells express distinct sets of miRNAs
- miR-17∼92 is upregulated upon stem cell activation in the adult V-SVZ
- miR-17∼92 affects proliferation, maturation, and fate in a lineage-dependent manner
- miR-17∼92 deletion impacts transit amplifying cell heterogeneity

Favaloro et al., 2022, Cell Reports *41*, 111773
December 6, 2022
https://doi.org/10.1016/j.celrep.2022.111773

Cell Reports

CellPress
OPEN ACCESS

Report

miR-17∼92 exerts stage-specific effects in adult V-SVZ neural stem cell lineages

Fabrizio Favaloro,[1,3] Annina M. DeLeo,[2,3] Ana C. Delgado,[1] and Fiona Doetsch[1,4,*]
[1]Biozentrum, University of Basel, 4056 Basel, Switzerland
[2]Department of Pathology and Cell Biology, Columbia University, New York, NY 10032, USA
[3]These authors contributed equally
[4]Lead contact
*Correspondence: fiona.doetsch@unibas.ch
https://doi.org/10.1016/j.celrep.2022.111773

SUMMARY

Neural stem cells (NSCs) in the adult ventricular-subventricular zone (V-SVZ) generate neurons and glia throughout life. MicroRNAs are important post-transcriptional regulators frequently acting in a context-dependent manner. Here, microRNA profiling defines cohorts of miRNAs in quiescent and activated NSCs, with miR-17∼92 highly upregulated in activated NSCs and transit amplifying cells (TACs) versus quiescent NSCs. Conditional miR-17∼92 deletion in the adult V-SVZ results in stage-specific effects. In NSCs, it reduces proliferation *in vitro* and *in vivo,* whereas in TACs, it selectively shifts neurogenic OLIG2$^-$ DLX2$^+$ toward oligodendrogenic OLIG2$^+$ DLX2$^-$ TACs, due to de-repression of an oligodendrogenic program, leading to increased oligodendrogenesis *in vivo*. This differential regulation of TAC subpopulations highlights the importance of TAC heterogeneity. Finally, in the NSC lineage for intraventricular oligodendrocyte progenitors, miR-17∼92 deletion decreases proliferation and maturation. Together, these findings reveal multiple stage-specific functions of the miR-17∼92 cluster within different adult V-SVZ lineages.

INTRODUCTION

In the adult mouse brain, the ventricular-subventricular zone (V-SVZ), adjacent to the lateral ventricles, is the largest germinal niche. V-SVZ NSCs are radial cells that express glial fibrillary acidic protein (GFAP). They are largely quiescent (qNSCs) and, upon activation (aNSCs), give rise to transit amplifying cells (TACs), which in turn generate neuroblasts that migrate to the olfactory bulb (OB) (Chaker et al., 2016; Obernier and Alvarez-Buylla, 2019). Importantly, NSCs also give rise to a small number of glial cells, including oligodendrocytes destined for the *corpus callosum* and intraventricular oligodendrocyte progenitor cells (OPCs) (Chaker et al., 2016; Delgado et al., 2021; Obernier and Alvarez-Buylla, 2019).

Cell transitions along the stem cell lineage are underlain by key changes in gene regulatory networks. microRNAs (miRNAs) are small non-coding RNAs that can rapidly sculpt cell transcriptomes by targeting hundreds of mRNA transcripts simultaneously (O'Brien et al., 2018). The regulation of adult NSC behavior by miRNAs is still little explored. Indeed, only a handful of miRNAs have been implicated in the regulation of adult V-SVZ neurogenesis and integration of OB neurons (Akerblom et al., 2014; Brett et al., 2011; Cheng et al., 2009; Coré et al., 2020; de Chevigny et al., 2012; Lepko et al., 2019; Liu et al., 2010; Pathania et al., 2012; Szulwach et al., 2010; Zhao et al., 2009, 2010). To expand the repertoire of miRNAs in the V-SVZ, we performed miRNA profiling of FACS-purified qNSCs, aNSCs and TACs and found miR-17∼92 significantly upregulated in aNSCs and TACs in comparison to qNSCs.

miR-17∼92 is a cluster of six co-transcribed miRNAs (-17, -18a, -19a and b, -20a, and -92a) with pleiotropic functions in several tissues during both development and tumorigenesis (Bian et al., 2013; Concepcion et al., 2012; Naka-Kaneda et al., 2014). In the adult V-SVZ, miR-17∼92 is up-regulated upon stroke where it induces proliferation and survival of progenitor cells (Liu et al., 2013). However, its role under homeostasis is unknown. Here, we show that miR-17∼92 not only regulates NSC proliferation, but also exerts multiple lineage and stage-specific effects within the adult V-SVZ.

RESULTS

miR-17∼92 is expressed in the adult V-SVZ neurogenic lineage

To identify miRNAs relevant to the early stages of the V-SVZ stem cell lineage we performed miRNA profiling of FACS-purified qNSCs, aNSCs and TACs (Codega et al., 2014; Pastrana et al., 2009) (Figure S1A) using Taqman miRNA arrays (Table S1). In addition to cohorts of miRNAs common to all three populations, we identified miRNAs that were differentially expressed in qNSCs and aNSCs. miR-30c, miR-26a, miR-99b, miR-193b, miR-30e, miR-129-3p and miR-145 were upregulated in qNSCs (Figure 1A). In contrast, all miRNAs significantly enriched in aNSCs over qNSCs were members of the miR-17∼92 cluster

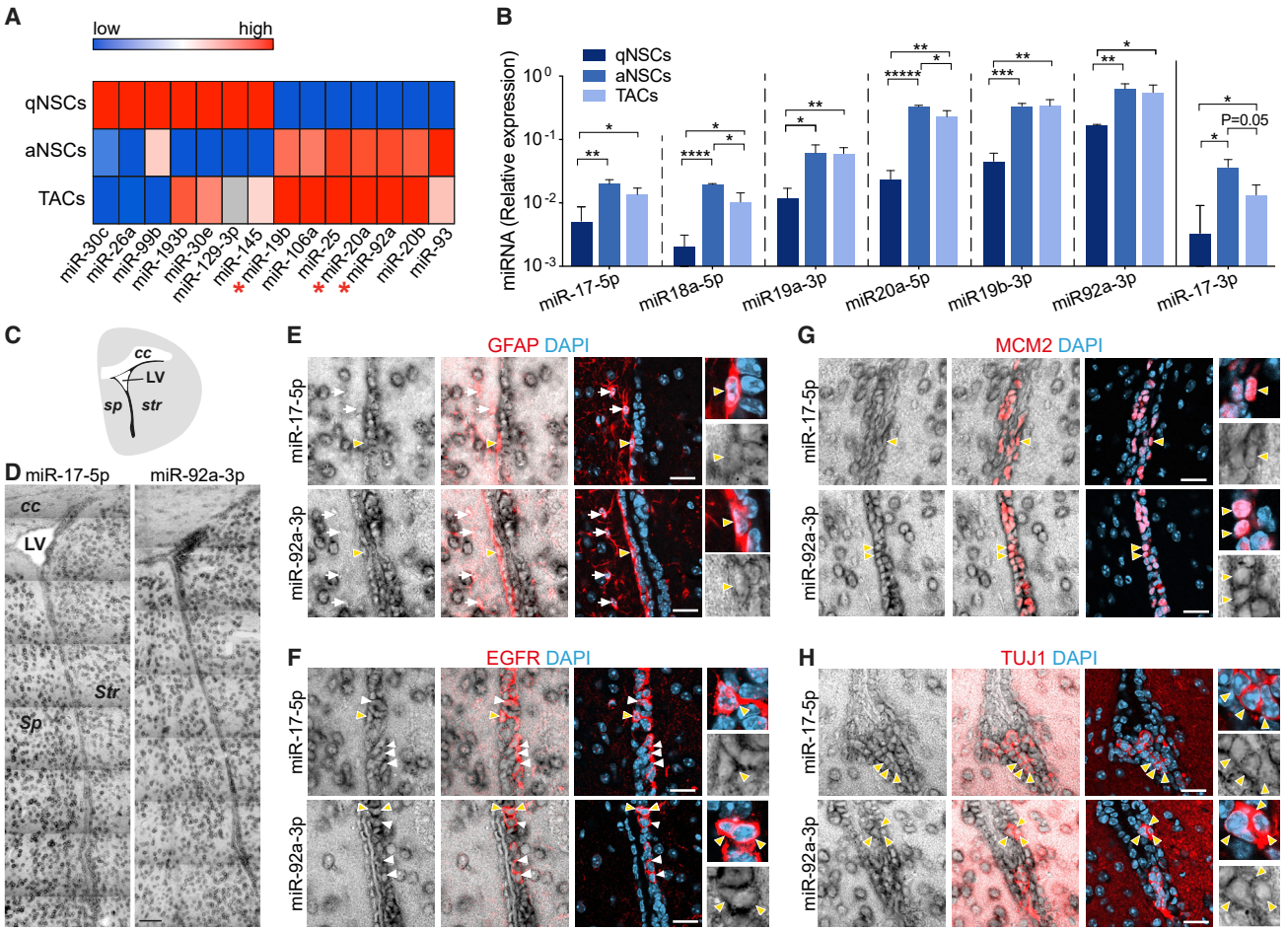

Figure 1. miR-17∼92 is expressed in the adult V-SVZ neurogenic lineage

(A) Heatmap of differentially expressed miRNAs between qNSCs and aNSCs. Asterisks indicate miR-17∼92 members.

(B) Relative expression ($2^{-\Delta Ct}$) of miR-17∼92 members in qNSCs, aNSCs and TACs (n = 3; mean ± SD). *p < 0.05, **p < 0.01, ***p < 0.001, ****p < 0.0001, and *****p < 0.00001.

(C) Coronal schema of brain hemisphere showing lateral ventricle (LV) and V-SVZ (black).

(D) *In situ* hybridization for miR-17-5p and miR-92a-3p in coronal sections.

(E–H) miR-17-5p (top) and miR-92a-3p (bottom) were expressed in a few GFAP$^+$ (red) radial cells (yellow arrowheads), but not in nearby astrocytes (white arrows) (E), in most EGFR$^+$ cells (red, arrowheads) (F), MCM2$^+$ cells (red) (G) and TUJ1$^+$ neuroblasts in the V-SVZ (red) (H). Yellow arrowheads indicate cells in high power images to the right. Scale bars: 20μm. *cc: corpus callosum, sp: septum, str: striatum*. See also Figure S1.

and its paralogs, miR-106a∼363 and miR-106b∼25 (Figure S1B), and were also expressed in TACs (Figure 1A). Here, we focused on the role of the miR-17∼92 cluster in the regulation of early stages of the adult V-SVZ lineage.

To confirm miR-17∼92 expression in the V-SVZ, we first performed qPCR analysis for mature miRNAs in FACS-purified cells. All guide forms of the miR-17∼92 cluster, as well as the star form miR-17-3p, were expressed at low levels in qNSCs and were significantly upregulated in both aNSCs and TACs (Figure 1B). *In situ* hybridization (ISH) revealed similar patterns throughout the V-SVZ for different members of the cluster, including miR-17-5p, miR-18-5p, miR-19a-3p and miR-92a-3p (Figures 1C, 1D, and S1C–S1E). All were broadly expressed without obvious regionality in the V-SVZ. However, individual miR-17∼92 members showed different levels of expression, with miR-92a-3p being the most abundant. To define which V-SVZ cells express the cluster, we combined ISH with immunostaining. Given the similar distribution of miR-17∼92 miRNAs, we focused on miR-17-5p and miR-92a-3p, the first and the last members of the cluster (Figure S1B). We detected miR-17-5p and miR-92a-3p in a few GFAP$^+$ radial cells (Figure 1E), consistent with their low level in FACS-purified qNSCs. In contrast, most proliferating cells, including MCM2$^+$ cells and epidermal growth factor receptor (EGFR)$^+$ TACs, had higher levels of miR-17-5p and miR-92a-3p (Figures 1F and 1G). TUJ1$^+$ neuroblasts also expressed miR-17-5p and miR-92a-3p (Figure 1H). Outside of the V-SVZ, cluster members were broadly detected throughout the brain (Figures 1D and S1C–S1E) in mature parenchymal neurons (Figure 1H) and in the choroid plexus (Figure S1E), but only rarely in astrocytes (glutamine synthetase$^+$ (GS) or GFAP$^+$) (Figures S1F and 1E). Thus, within the V-SVZ, the miR-17∼92

CellPress
OPEN ACCESS

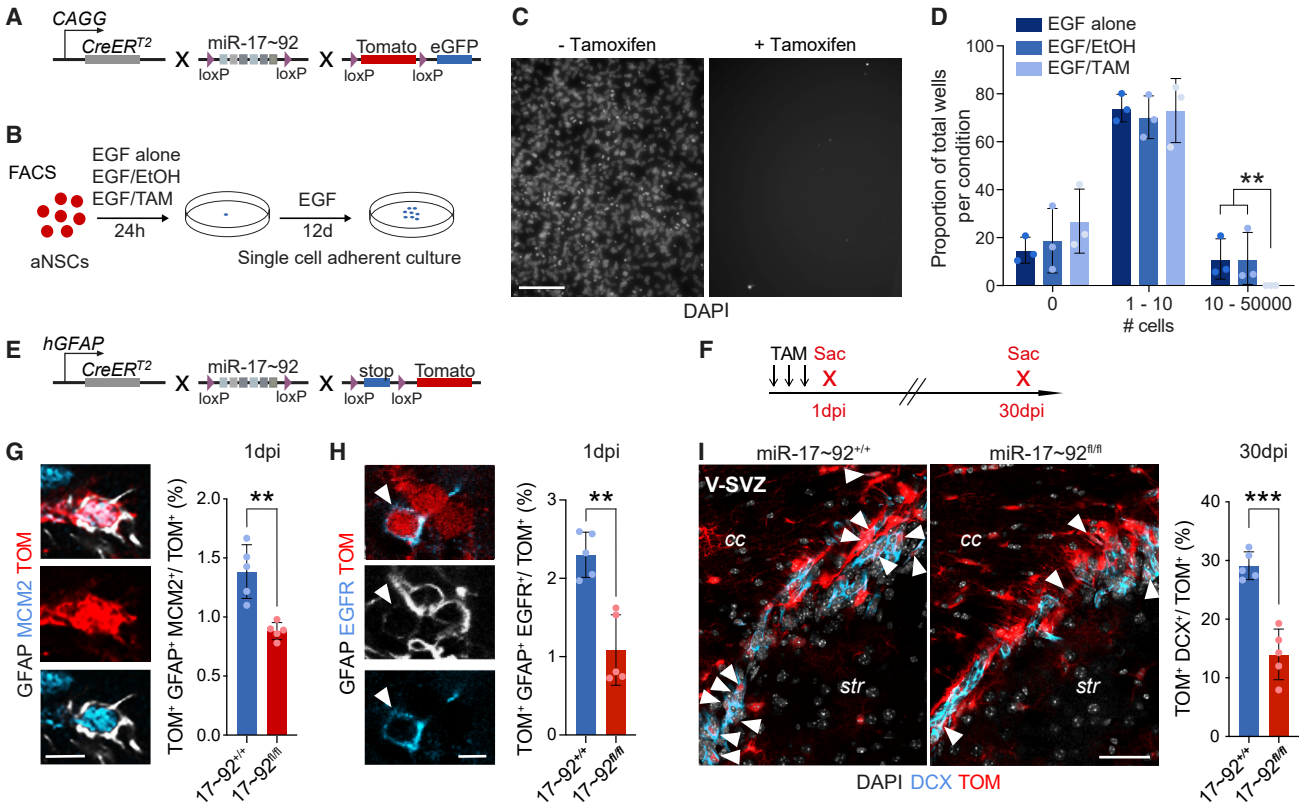

Figure 2. miR-17∼92 deletion in NSCs reduces stem cell proliferation and neurogenesis

(A and B) (A) Schematic of mouse line and (B) experimental paradigm for miR-17∼92 deletion *in vitro*.

(C) Representative images and (D) quantification (DAPI$^+$ cells) of single cell aNSC adherent cultures from CAGG-miR-17∼92$^{fl/fl}$ control (left) and deleted cells (right) (n = 3; mean ± SD).

(E) Schematic of mouse line and (F) experimental paradigm for miR-17∼92 deletion *in vivo*.

(G and H) Confocal images and quantification of V-SVZ TOM$^+$ GFAP$^+$ MCM2$^+$ NSCs (G) and TOM$^+$ GFAP$^+$ EGFR$^+$ NSCs (H, arrowheads) at 1dpi, and TOM$^+$ DCX$^+$ neuroblasts (I) at 30dpi (n = 5; mean ± SD). Data points represent individual experiments (D) or mice (G–I). **p < 0.01 and ***p < 0.001. Scale bars: (G and H) 5μm, (I) 20μm, (C) 100μm. cc: *corpus callosum*, str: *striatum*. See also Figure S2.

cluster is upregulated upon stem cell activation and is expressed along the neurogenic lineage.

miR-17∼92 deletion reduces NSC proliferation and neurogenesis

To assess the effect of miR-17∼92 deletion on NSCs *in vitro*, we FACS-purified aNSCs from adult CAGG::CreER$^{T2+/-}$; miR-17∼92$^{fl/fl}$; ROSA$^{(ACTB\text{-}tdTomato,\text{-}EGFP)}$ (CAGG-miR-17∼92$^{fl/fl}$) mice, in which miR-17∼92 is deleted upon addition of hydroxytamoxifen, and reporter expression is switched from tdTomato to eGFP (Figure 2A). We confirmed successful deletion of the whole miR-17∼92 cluster *in vitro* (Figures S2A and B). In single cell adherent cultures, miR-17∼92-deleted cells exhibited little proliferation and failed to generate large colonies (>10 cells) as opposed to their control counterparts that gave rise to large clones (>500 cells) (Figures 2B–2D). Despite a role for miR-17∼92 in cell survival (Koralov et al., 2008; Olive et al., 2009, 2010; Tung et al., 2015; Ventura et al., 2008; Xiao et al., 2008), this lack of large colonies was not due to increased apoptosis based on Annexin staining (Figure S2C). Deletion of the cluster in FACS-purified aNSCs also resulted in fewer and visibly smaller primary neurospheres (Figures S2D–S2F). Together, these results show an important function of the cluster in adult NSC proliferation *in vitro*.

To investigate the role of miR-17∼92 in V-SVZ NSCs and their lineage *in vivo,* we selectively deleted the cluster in GFAP$^+$ NSCs. Adult hGFAP::CreERT2$^{+/+}$; miR-17∼92$^{+/+}$; Ai14 (miR-17∼92$^{+/+}$) and hGFAP::CreER$^{T2+/+}$; miR-17∼92$^{fl/fl}$; Ai14 (miR-17∼92$^{fl/fl}$) mice, in which administration of tamoxifen (TAM) induces miR-17∼92 deletion and initiates tdTomato reporter expression in GFAP$^+$ cells (Figure 2E), were analyzed 1 and 30 days post TAM injections (dpi) (Figure 2F). qPCR analysis of FACS-purified Tomato$^+$ (TOM) EGFR$^+$ cells (aNSCs and TACs) confirmed deletion of miR-17∼92 at 1dpi *in vivo* (Figures S2G and S2H). At both time points, the average number of TOM$^+$ cells per V-SVZ section was unchanged between control and deleted mice (Figures S3A and S3B). However, due to variable levels of recombination in individual mice, we report all data as proportions.

Deletion of the cluster at 1dpi also reduced the proportion of dividing NSCs (GFAP$^+$ MCM2$^+$) *in vivo* (Figure 2G). To assess

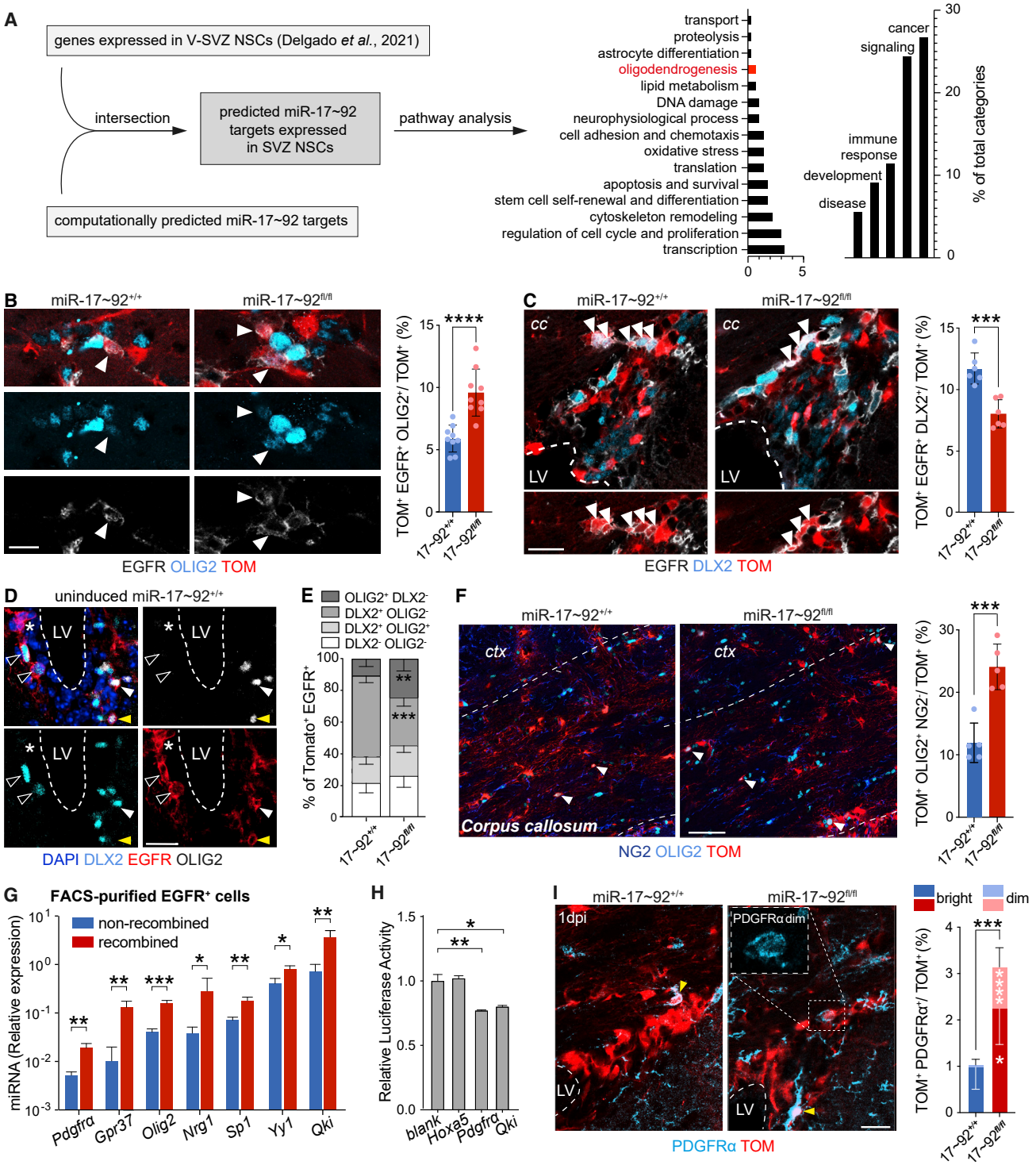

Figure 3. miR-17∼92 deletion shifts neurogenic to oligodendrogenic transit amplifying cells by de-repressing an oligodendrogenic program

(A) Flowchart of bioinformatic analysis to identify predicted miR-17∼92 targets in V-SVZ NSCs (left) and their top-enriched pathways (MetaCore) (right).

(B and C) Confocal images and quantification of TOM$^+$ EGFR$^+$ OLIG2$^+$ TACs (arrowheads) (n = 9; mean ± SD) (B) and TOM$^+$ EGFR$^+$ DLX2$^+$ TACs (arrowheads) (n = 6; mean ± SD) (C) at 1dpi.

(D) Confocal micrographs of EGFR (red), DLX2 (blue) and OLIG2 (white) staining on uninduced control miR-17∼92$^{+/+}$ mice showing triple positive cell (white arrowheads), EGFR$^+$ DLX2$^+$ OLIG2$^-$ cells (empty arrowheads), EGFR$^+$ DLX2$^-$ OLIG2$^-$ cell (asterisks) and EGFR$^+$ DLX2$^-$ OLIG2$^+$ cell (yellow arrowheads).

(E) Quantification of different TAC (TOM$^+$ EGFR$^+$) populations at 1dpi (n = 5; mean ± SD).

(legend continued on next page)

if proliferation was affected at each stage of the lineage, we immunostained for GFAP and EGFR to discriminate between aNSCs (GFAP$^+$ EGFR$^+$) and TACs (GFAP$^-$ EGFR$^+$), and DCX to label neuroblasts, together with the proliferation marker Ki67 (Figure S3C). Deletion of the cluster decreased the overall proportion of aNSCs among the total TOM$^+$ population (Figure 2H) as well as the proportion of aNSCs expressing Ki67 (Figure S3D). In contrast, neither the total proportion of, nor Ki67$^+$ cells among, TACs or neuroblasts were affected at 1dpi (Figures S3D–S3F). Apoptotic cells (Caspase 3, CASP3$^+$) (Figure S3G) were also unchanged at 1dpi *in vivo*. Importantly, no changes were detected in TOM$^-$ cells, indicating that the effects we observed in the stem cell lineage are cell autonomous (Figures S3I–S3M), unlike in tumors where miR-19a-containing exosomes can be released by astrocytes (Zhang et al., 2015). Thirty days after cluster deletion, the proportion of TOM$^+$ qNSCs in the V-SVZ was increased, paralleled by a decrease in TOM$^+$ aNSCs, consistent with reduced stem cell activation (Figures S3N–S3Q). DCX$^+$ neuroblasts were also decreased at 30dpi (Figure 2I). In sum, miR-17∼92 deletion in NSCs *in vivo* decreases NSC proliferation and neurogenesis in the V-SVZ.

miR-17∼92 targets are enriched in stem cell and gliogenesis-related pathways

To investigate additional roles for miR-17∼92 in the adult V-SVZ, we performed bioinformatic analysis by comparing predicted miR-17∼92 targets to genes expressed in adult V-SVZ NSCs (Delgado et al., 2021) followed by pathway analysis (Figure 3A). As previously reported, the majority of miR-17∼92 targets were in gene categories related to 'cancer', 'immune response', 'development' and 'apoptosis and survival' (Figure 3A and Table S2) (Concepcion et al., 2012; Han et al., 2015; Olive et al., 2010; Ventura et al., 2008; Xu et al., 2015). In addition, miR-17∼92 targets were found in categories enriched in qNSCs, such as 'cell adhesion' and 'lipid metabolism', and aNSCs, such as 'regulation of cell cycle and proliferation' and 'stem cell self-renewal and differentiation' (Baser et al., 2019; Codega et al., 2014; Delgado et al., 2021; Llorens-Bobadilla et al., 2015). Interestingly, pathway analysis also identified targets related to 'astrocyte differentiation' and 'oligodendrogenesis', including the master regulator of oligodendrogenesis *Olig2*. As such, miR-17∼92 may also regulate neurogenesis within the adult V-SVZ by repressing gliogenesis.

miR-17∼92 deletion shifts neurogenic to oligodendrogenic transit amplifying cells and increases oligodendrogenesis *in vivo*

The majority of newly born cells in the adult V-SVZ are neuroblasts, generated by DLX2$^+$ TACs (Anderson et al., 1997; Brill et al., 2008; Doetsch et al., 2002). However, the V-SVZ also generates oligodendrocytes destined for the *corpus callosum*, via OLIG2$^+$ TACs (Menn et al., 2006; Nait-Oumesmar et al., 1999; Ortega et al., 2013). Importantly, over-expression and knock-out of *Dlx2* or *Olig2* is sufficient to shift progenitor cells into a neurogenic or oligodendrogenic fate respectively (Boshans et al., 2021; Jiang et al., 2020; Petryniak et al., 2007). Given the enrichment of miR-17∼92 targets in 'oligodendrogenesis', we focused on whether cluster deletion results in a shift towards oligodendrogenesis in the adult V-SVZ.

Olig2 is a functional miR-17∼92 target during development (Chen et al., 2011). We postulated that if *Olig2* is also a target in the adult V-SVZ, OLIG2 would increase upon miR-17∼92 deletion. We therefore immunostained for OLIG2 together with GFAP and EGFR at 1dpi. Deletion of the cluster did not affect the proportion of OLIG2$^+$ aNSCs (Figure S3H). Notably, although the proportion of total TACs (Figure S3E) did not change, miR-17∼92 deletion resulted in an increase in TACs expressing OLIG2 (Figure 3B). Conversely, cluster deletion reduced neurogenic TACs (EGFR$^+$ DLX2$^+$) (Figure 3C).

To better understand how TACs are affected by miR-17∼92 deletion, we performed co-immunostaining for EGFR, DLX2 and OLIG2. We identified four subpopulations of EGFR$^+$ TACs based on OLIG2 and DLX2 expression, revealing unexpected heterogeneity. As previously described (Doetsch et al., 2002; Menn et al., 2006), we detected neurogenic (DLX2$^+$ OLIG2$^-$) (46% ± 2.5%) and oligodendrogenic (OLIG2$^+$ DLX2$^-$) (24.5% ± 1%) TACs (Figures 3D, S4A, and S4B). We also identified a smaller proportion of TACs co-expressing DLX2 and OLIG2 (13.5% ± 1.1%), and one negative for both markers (16% ± 2.2%) (Figures 3D, S4A, and S4B). At 1dpi, miR-17∼92 deletion did not change the proportion of OLIG2$^+$ DLX2$^+$ TACs or double negative TACs (Figure 3E). Instead, deletion of the cluster led to an increase in the proportion of OLIG2$^+$ DLX2$^-$ and a decrease in DLX2$^+$ OLIG2$^-$ TACs (Figure 3E). Thus, the global increase in OLIG2$^+$ TACs was due to a selective shift from neurogenic toward oligodendrogenic TACs. Consistent with this shift, mature oligodendrocytes (OLIG2$^+$ NG2$^-$) were increased in the *corpus callosum* in miR-17∼92 deleted mice at 30 dpi (Figure 3F).

To identify additional oligodendrogenic targets regulated by miR-17∼92 we examined candidates revealed by our pathway analysis, including *Pdgfrα, Gpr37, Olig2, Nrg1, Sp1, Yy1* and *Qki* by qPCR 1dpi after miR-17∼92 deletion. All were significantly upregulated (Figure 3G). We further validated *Pdgfrα* and *Qki* as biochemical targets using luciferase assays (Figure 3H). Moreover, PDGFRα was upregulated in deleted cells *in vivo* at 1dpi, largely due to an increase in PDGFRα dim cells, which are rare in control mice (Figure 3I). Finally, *in vitro* differentiation of neurospheres after deletion of the cluster led to a significant reduction in TUJ1$^+$ neurons (Figures S4C and S4D) and a significant increase in O4$^+$ oligodendrocytes (Figures S4C and

(F) Confocal images and quantification of TOM$^+$ OLIG2$^+$ NG2$^-$ cells in the *corpus callosum* at 30dpi (n = 5; mean ± SD).
(G) Relative expression of oligodendrogenesis-related miR-17∼92 targets in FACS-purified cells (n = 3; mean ± SD).
(H) Luciferase reporter assay of miR-17∼92 targets and *Hoxa5* non-targeted negative control (Tung et al., 2015) (n = 3; mean ± SD).
(I) Confocal images and quantification of TOM$^+$ PDGFRα$^+$ cells (arrowheads indicate bright cells) at 1dpi (n = 5; mean ± SD). Data points represent individual mice. $^*p < 0.05$, $^{**}p < 0.01$, $^{***}p < 0.001$, and $^{****}p < 0.0001$. Scale bar: (B and C) 10μm, (D and I) 20μm, (F) 50μm. cc: *corpus callosum*, ctx: *cortex*, LV: lateral ventricle. See also Figures S3 and S4.

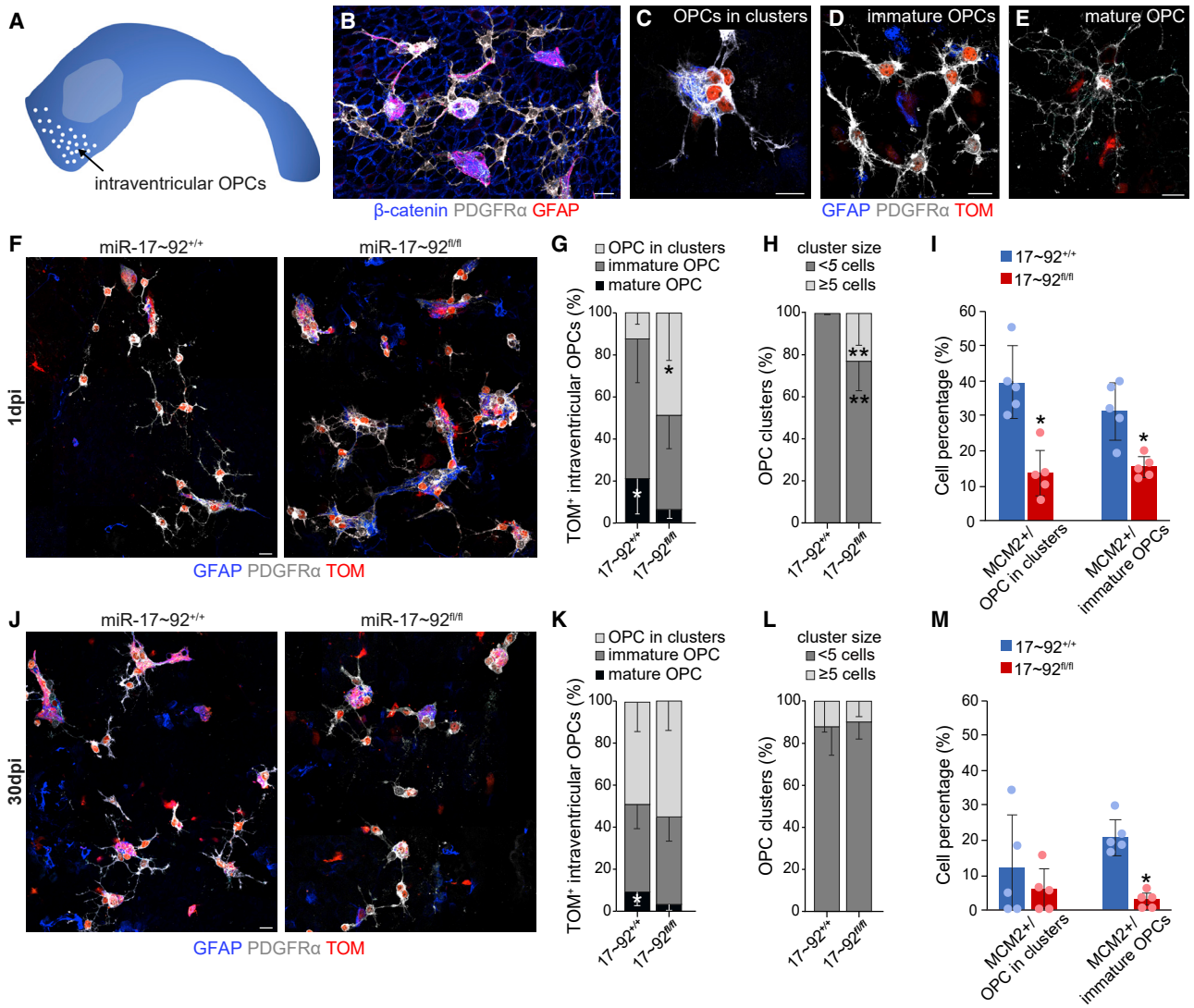

Figure 4. miR-17∼92 regulates intraventricular OPC proliferation and maturation

(A) Wholemount schema showing location of intraventricular OPCs (white dots).

(B–E) Low (B) and high power confocal images (C–E) of PDGFRα$^+$ intraventricular OPCs on top of ventricular surface (β-catenin) at different maturation stages.

(F–M) Confocal images of wholemounts (F and J) and quantification of intraventricular OPCs at different maturation stages (G and K), large (≥5 cells) and small (<5 cells) OPC clusters (H and L), and MCM2$^+$ cells at different stages (I and M) at 1 (F–I) and 30dpi (J–M) (n ≥ 5; mean ± SD). Data points represent individual mice. *p < 0.05 and **p < 0.01. Scale bars: 10μm. See also Figure S4.

S4E). Altogether, these results highlight a role for the miR-17∼92 cluster in repressing an oligodendrogenic program within the V-SVZ.

miR-17∼92 regulates intraventricular OPC proliferation and maturation

V-SVZ NSCs also generate intraventricular oligodendrocyte progenitors (OPCs), located on the surface of the lateral ventricle walls, via a distinct lineage (Delgado et al., 2021) (Figures 4A and 4B). Intraventricular OPCs arise in GFAP$^+$ clusters (OPCs in clusters) (Figure 4C), then disperse from the clusters as immature cells with few processes (immature OPCs) (Figure 4D), and mature to have more a ramified morphology (mature OPCs) (Figure 4E). miR-17∼92 deletion also reduced the proportion of intraventricular OPCs expressing MCM2 at 1dpi and 30dpi (Figures 4I, 4M, S4F, and S4G). Interestingly, at 1dpi, more TOM$^+$ OPCs were present in clusters in mutant mice compared to controls (50% versus 15%) (Figures 4F and 4G) and more of the clusters were larger (>5 cells) (Figures 4F and 4H). This increased cluster size was not due to increased proliferation (Figures 4I and S4F) or to defects in survival, as no CASP3$^+$ intraventricular OPCs were detected (Figures S4H and S4I). Instead, it was likely due to impaired OPC maturation, as the proportion of mature intraventricular OPCs was significantly decreased in

mutant mice compared to controls at both 1dpi and 30dpi (Figures 4F, 4G, 4J, and 4K). Thus, our results uncover a role for the miR-17∼92 cluster in the regulation of intraventricular OPC proliferation and maturation.

DISCUSSION

miRNAs are emerging as important regulators of adult NSCs. Here, we identify differentially expressed miRNA candidates in both qNSCs and aNSCs. These distinct miRNA cohorts reflect the existence of different gene regulatory networks underlying qNSC and aNSC states. Our findings also uncover multiple roles for the miR-17∼92 cluster in the regulation of the adult V-SVZ stem cell lineages, highlighting its key contribution to the dynamics of this adult stem cell niche.

Some of the functions of miR-17∼92 are shared across diverse tissue compartments and developmental processes. Proliferation is the best known role of miR-17∼92 in multiple organs during embryogenesis and adulthood, as well as in cancers (Mavrakis et al., 2010; Mu et al., 2009; Olive et al., 2009; Ventura et al., 2008), and is often modulated by miR-17∼92 in parallel with other processes. Indeed, within the developing brain, miR-17∼92 concomitantly promotes the expansion of radial glial cells and prevents their premature transition into intermediate progenitors (Bian et al., 2013; Chen et al., 2014; Fei et al., 2014). Moreover, it also sustains the neurogenic phase by inhibiting acquisition of gliogenic competence and repressing astrocytogenesis (Mao et al., 2014; Naka-Kaneda et al., 2014). miR-17∼92 can also regulate cell survival in different contexts in both normal and pathological conditions (Koralov et al., 2008; Liu et al., 2013; Olive et al., 2009, 2010; Tung et al., 2015; Ventura et al., 2008; Xiao et al., 2008).

Here we show that, within the V-SVZ under homeostasis, miR-17∼92 is upregulated upon stem cell activation and its expression is maintained in TACs and in neuroblasts. In addition to promoting stem cell proliferation, the cluster actively represses an oligodendrogenic program in neurogenic transit amplifying cells. miR-17∼92 also acts in the V-SVZ lineage that generates intraventricular OPCs, promoting their proliferation and acquisition of a mature morphology. However, miR-17∼92 has no pro-survival function at early stages in these different lineages. These multiple and diverse roles likely reflect the different ensembles of targets expressed in a cell type and context-specific manner.

Unlike the well-described heterogeneity of adult V-SVZ NSCs, including their developmental origins (Fuentealba et al., 2015; Furutachi et al., 2015; Yuzwa et al., 2017), morphology (Delgado et al., 2021; Mirzadeh et al., 2008; Shen et al., 2008), regional position (reviewed in Azim et al. (2016) and response to physiological cues (Chaker et al., 2021; Paul et al., 2017), the heterogeneity among TACs is less explored. TACs have different cell cycle lengths (Ponti et al., 2013) and at early postnatal stages, TACs in the dorsal V-SVZ (roof of the ventricle) differ in their transcriptional signatures from those in the lateral wall (Azim et al., 2015). Here, our findings show that multiple subpopulations of TACs can be distinguished based on the exclusive, concomitant or lack of expression of DLX2 and OLIG2 proteins, two key neurogenic and oligodendrogenic transcription factors. As adult V-SVZ NSCs generate many different types of neurons as well as glial progeny, it will be interesting to assess how many subtypes of TACs exist, and their lineage relationships. While TACs co-expressing transcription factors for different lineages may be earlier in the stem cell lineage and correspond to a more multipotent primed TAC, those lacking both DLX2 and OLIG2 may be progenitors for astrocytes, which are also generated within the V-SVZ (Delgado et al., 2021; Sohn et al., 2015). How this diversity of transcription factor expression extends to receptor and signaling pathway effectors will be interesting to uncover. Our findings suggest that fate decisions are also made at the level of TACs, and not only NSCs, and that miRNAs are well-poised to modulate multiple stages of the adult stem cell lineage.

miR-17∼92 has been implicated in numerous disorders, including cancer (Concepcion et al., 2012; de Pontual et al., 2011; Hayashita et al., 2005; He et al., 2005; Mi et al., 2010; Ota et al., 2004), anxiety and depression (Jin et al., 2016) and is upregulated upon stroke (Liu et al., 2013). The lineage and cell-type specific effects of the cluster in the adult V-SVZ we have uncovered suggest that modulation of miR-17∼92 may be an important mechanism to dynamically fine-tune the generation of distinct neurogenic and gliogenic lineages from adult neural stem cells in response to different physiological and pathological contexts. As such, miR-17∼92 may be downregulated during demyelination, when oligodendrogenesis is increased. Altogether, our findings highlight that miRNAs are important components of the complex multi-layered regulation of adult V-SVZ NSCs and their lineages.

Limitations of the study

In this study we have deleted the entire miR-17∼92 cluster. As such, the specific contribution of individual miR-17∼92 miRNAs, as well as the miR-17∼92 paralogues miR-106a∼363 and miR-106b∼25 to adult V-SVZ regulation, has not been dissected.

STAR★METHODS

Detailed methods are provided in the online version of this paper and include the following:

- KEY RESOURCES TABLE
- RESOURCE AVAILABILITY
  - Lead contact
  - Materials availability
  - Data and code availability
- EXPERIMENTAL MODEL AND SUBJECT DETAILS
  - Mice
- METHOD DETAILS
  - FACS-purification strategy
  - miRNA profiling and qPCR analysis
  - *In vitro* assays
  - Tamoxifen injections
  - Validation of miR-17∼92 deletion and targets
  - Tissue preparation
  - miRNA *in situ* hybridization
  - Immunostaining
  - Antibodies
  - Brain section imaging and quantification

SUPPLEMENTAL INFORMATION

Supplemental information can be found online at https://doi.org/10.1016/j.celrep.2022.111773.

ACKNOWLEDGMENTS

Work was supported by NIH NINDS R01 NS074039, NIH NINDS R01NS053884, NIH NINDS ARRA NS053884-03S109, NYSTEM C028118, NYSTEM C024287, Swiss National Science Foundation 31003A_163088, European Research Council Advanced Grant (No 789328), and the University of Basel to FD, and NIH T32 GM008224, TL1 TR000082 and NIH NINDS F31NS081990 (A.M.D.). We thank members of the Doetsch and Wichterle labs, J.A. Chen, H. Wichterle, P. Scheiffele and J. Betschinger for discussion; P. Codega, E. Pastrana, V. Crotet and V. Silva-Vargas for help with experiments; K. Gordon and S. Tetteh of the Herbert Irving Comprehensive Cancer Center of Columbia University for assistance with FACS; J. Zavadil at the Genome Technology Center of NYU Langone Medical Center; the Biozentrum Imaging Core Facility and L. Guérard for help with automated quantification; J. Bögli and S. Stefanova at the Biozentrum FACS Core Facility. We thank J. Chen, H. Wichterle and L. Jeker for mouse lines, J.A. Chen for the Hoxa5 luciferase construct, T. Sun for sharing the *in situ* hybridization protocol, and C. Schindler for help with statistical analysis.

AUTHOR CONTRIBUTIONS

Conceptualization: F.D., F.F., and A.D. Performed experiments: F.F., A.D., and A.C.D. Data analysis: F.F., A.D., and A.C.D. Supervision: F.D. Manuscript writing: F.D. and F.F.

DECLARATION OF INTERESTS

The authors declare no competing interests.

INCLUSION AND DIVERSITY

We support inclusive, diverse, and equitable conduct of research.

Received: July 27, 2021
Revised: June 11, 2022
Accepted: November 14, 2022
Published: December 6, 2022

REFERENCES

Akerblom, M., Petri, R., Sachdeva, R., Klussendorf, T., Mattsson, B., Gentner, B., and Jakobsson, J. (2014). microRNA-125 distinguishes developmentally generated and adult-born olfactory bulb interneurons. Development *141*, 1580–1588. https://doi.org/10.1242/dev.101659.

Anderson, S.A., Qiu, M., Bulfone, A., Eisenstat, D.D., Meneses, J., Pedersen, R., and Rubenstein, J.L. (1997). Mutations of the homeobox genes Dlx-1 and Dlx-2 disrupt the striatal subventricular zone and differentiation of late born striatal neurons. Neuron *19*, 27–37. https://doi.org/10.1016/s0896-6273(00)80345-1.

Azim, K., Berninger, B., and Raineteau, O. (2016). Mosaic subventricular origins of forebrain oligodendrogenesis. Front. Neurosci. *10*, 107. https://doi.org/10.3389/fnins.2016.00107.

Azim, K., Hurtado-Chong, A., Fischer, B., Kumar, N., Zweifel, S., Taylor, V., and Raineteau, O. (2015). Transcriptional hallmarks of heterogeneous neural stem cell niches of the subventricular zone. Stem Cell. *33*, 2232–2242. https://doi.org/10.1002/stem.2017.

Baser, A., Skabkin, M., Kleber, S., Dang, Y., Gülcüler Balta, G.S., Kalamakis, G., Göpferich, M., Ibañez, D.C., Schefzik, R., Lopez, A.S., et al. (2019). Onset of differentiation is post-transcriptionally controlled in adult neural stem cells. Nature *566*, 100–104. https://doi.org/10.1038/s41586-019-0888-x.

Belenguer, G., Domingo-Muelas, A., Ferrón, S.R., Morante-Redolat, J.M., and Fariñas, I. (2016). Isolation, culture and analysis of adult subependymal neural stem cells. Differentiation *91*, 28–41. https://doi.org/10.1016/j.diff.2016.01.005.

Bian, S., Hong, J., Li, Q., Schebelle, L., Pollock, A., Knauss, J.L., Garg, V., and Sun, T. (2013). MicroRNA cluster miR-17-92 regulates neural stem cell expansion and transition to intermediate progenitors in the developing mouse neocortex. Cell Rep. *3*, 1398–1406. https://doi.org/10.1016/j.celrep.2013.03.037.

Boshans, L.L., Soh, H., Wood, W.M., Nolan, T.M., Mandoiu, I.I., Yanagawa, Y., Tzingounis, A.V., and Nishiyama, A. (2021). Direct reprogramming of oligodendrocyte precursor cells into GABAergic inhibitory neurons by a single homeodomain transcription factor Dlx2. Sci. Rep. *11*, 3552. https://doi.org/10.1038/s41598-021-82931-9.

Brett, J.O., Renault, V.M., Rafalski, V.A., Webb, A.E., and Brunet, A. (2011). The microRNA cluster miR-106b∼25 regulates adult neural stem/progenitor cell proliferation and neuronal differentiation. Aging *3*, 108–124. https://doi.org/10.18632/aging.100285.

Brill, M.S., Snapyan, M., Wohlfrom, H., Ninkovic, J., Jawerka, M., Mastick, G.S., Ashery-Padan, R., Saghatelyan, A., Berninger, B., and Götz, M. (2008). A Dlx2- and Pax6-dependent transcriptional code for periglomerular neuron specification in the adult olfactory bulb. J. Neurosci. *28*, 6439–6452. https://doi.org/10.1523/jneurosci.0700-08.2008.

Chaker, Z., Codega, P., and Doetsch, F. (2016). A mosaic world: puzzles revealed by adult neural stem cell heterogeneity. Wiley Interdiscip. Rev. Dev. Biol. *5*, 640–658. https://doi.org/10.1002/wdev.248.

Chaker, Z., Segalada, C., and Doetsch, F. (2021). Spatio-temporal recruitment of adult neural stem cells for transient neurogenesis during pregnancy. Preprint at bioRxiv. https://doi.org/10.1101/2021.07.11.451957.

Chen, J.A., Huang, Y.P., Mazzoni, E.O., Tan, G.C., Zavadil, J., and Wichterle, H. (2011). Mir-17-3p controls spinal neural progenitor patterning by regulating Olig2/Irx3 cross-repressive loop. Neuron *69*, 721–735. https://doi.org/10.1016/j.neuron.2011.01.014.

Chen, Y., Bian, S., Zhang, J., Zhang, H., Tang, B., and Sun, T. (2014). The silencing effect of microRNA miR-17 on p21 maintains the neural progenitor pool in the developing cerebral cortex. Front. Neurol. *5*, 132. https://doi.org/10.3389/fneur.2014.00132.

Cheng, L.C., Pastrana, E., Tavazoie, M., and Doetsch, F. (2009). miR-124 regulates adult neurogenesis in the subventricular zone stem cell niche. Nat. Neurosci. *12*, 399–408. https://doi.org/10.1038/nn.2294.

Codega, P., Silva-Vargas, V., Paul, A., Maldonado-Soto, A.R., Deleo, A.M., Pastrana, E., and Doetsch, F. (2014). Prospective identification and purification of quiescent adult neural stem cells from their in vivo niche. Neuron *82*, 545–559. https://doi.org/10.1016/j.neuron.2014.02.039.

Concepcion, C.P., Bonetti, C., and Ventura, A. (2012). The microRNA-17-92 family of microRNA clusters in development and disease. Cancer J. *18*, 262–267. https://doi.org/10.1097/PPO.0b013e318258b60a.

Coré, N., Erni, A., Hoffmann, H.M., Mellon, P.L., Saurin, A.J., Beclin, C., and Cremer, H. (2020). Stem cell regionalization during olfactory bulb neurogenesis depends on regulatory interactions between Vax1 and Pax6. Elife *9*, e58215. https://doi.org/10.7554/eLife.58215.

de Chevigny, A., Coré, N., Follert, P., Gaudin, M., Barbry, P., Béclin, C., and Cremer, H. (2012). miR-7a regulation of Pax6 controls spatial origin of forebrain dopaminergic neurons. Nat. Neurosci. *15*, 1120–1126. https://doi.org/10.1038/nn.3142.

de Pontual, L., Yao, E., Callier, P., Faivre, L., Drouin, V., Cariou, S., Van Haeringen, A., Geneviève, D., Goldenberg, A., Oufadem, M., et al. (2011). Germline

deletion of the miR-17∼92 cluster causes skeletal and growth defects in humans. Nat. Genet. *43*, 1026–1030. https://doi.org/10.1038/ng.915.

Delgado, A.C., Maldonado-Soto, A.R., Silva-Vargas, V., Mizrak, D., von Känel, T., Tan, K.R., Paul, A., Madar, A., Cuervo, H., Kitajewski, J., et al. (2021). Release of stem cells from quiescence reveals gliogenic domains in the adult mouse brain. Science *372*, 1205–1209. https://doi.org/10.1126/science.abg8467.

Doetsch, F., Petreanu, L., Caille, I., Garcia-Verdugo, J.-M., and Alvarez-Buylla, A. (2002). EGF converts transit-amplifying neurogenic precursors in the adult brain into multipotent stem cells. Neuron *36*, 1021–1034. https://doi.org/10.1016/s0896-6273(02)01133-9.

Eriksen, A.H.M., Andersen, R.F., Pallisgaard, N., Sørensen, F.B., Jakobsen, A., and Hansen, T.F. (2016). MicroRNA expression profiling to identify and validate reference genes for the relative quantification of microRNA in rectal cancer. PLoS One *11*, e0150593. https://doi.org/10.1371/journal.pone.0150593.

Fei, J.F., Haffner, C., and Huttner, W.B. (2014). 3' UTR-dependent, miR-92-mediated restriction of Tis21 expression maintains asymmetric neural stem cell division to ensure proper neocortex size. Cell Rep. *7*, 398–411. https://doi.org/10.1016/j.celrep.2014.03.033.

Fuentealba, L.C., Rompani, S.B., Parraguez, J.I., Obernier, K., Romero, R., Cepko, C.L., and Alvarez-Buylla, A. (2015). Embryonic origin of postnatal neural stem cells. Cell *161*, 1644–1655. https://doi.org/10.1016/j.cell.2015.05.041.

Furutachi, S., Miya, H., Watanabe, T., Kawai, H., Yamasaki, N., Harada, Y., Imayoshi, I., Nelson, M., Nakayama, K.I., Hirabayashi, Y., and Gotoh, Y. (2015). Slowly dividing neural progenitors are an embryonic origin of adult neural stem cells. Nat. Neurosci. *18*, 657–665. https://doi.org/10.1038/nn.3989.

Han, Y.C., Vidigal, J.A., Mu, P., Yao, E., Singh, I., González, A.J., Concepcion, C.P., Bonetti, C., Ogrodowski, P., Carver, B., et al. (2015). An allelic series of miR-17 approximately 92-mutant mice uncovers functional specialization and cooperation among members of a microRNA polycistron. Nat. Genet. *47*, 766–775. https://doi.org/10.1038/ng.3321.

Hayashita, Y., Osada, H., Tatematsu, Y., Yamada, H., Yanagisawa, K., Tomida, S., Yatabe, Y., Kawahara, K., Sekido, Y., and Takahashi, T. (2005). A polycistronic microRNA cluster, miR-17-92, is overexpressed in human lung cancers and enhances cell proliferation. Cancer Res. *65*, 9628–9632. https://doi.org/10.1158/0008-5472.Can-05-2352.

He, L., Thomson, J.M., Hemann, M.T., Hernando-Monge, E., Mu, D., Goodson, S., Powers, S., Cordon-Cardo, C., Lowe, S.W., Hannon, G.J., and Hammond, S.M. (2005). A microRNA polycistron as a potential human oncogene. Nature *435*, 828–833. https://doi.org/10.1038/nature03552.

Jiang, Q., Zagozewski, J., Godbout, R., and Eisenstat, D.D. (2020). Distal-less genes *Dlx1*/*Dlx2* repress oligodendrocyte genesis through transcriptional inhibition of *Olig2* expression in the developing vertebrate forebrain. Preprint at bioRxiv. https://doi.org/10.1101/2020.04.09.012385.

Jin, J., Kim, S.N., Liu, X., Zhang, H., Zhang, C., Seo, J.S., Kim, Y., and Sun, T. (2016). miR-17-92 cluster regulates adult hippocampal neurogenesis, anxiety, and depression. Cell Rep. *16*, 1653–1663. https://doi.org/10.1016/j.celrep.2016.06.101.

Koralov, S.B., Muljo, S.A., Galler, G.R., Krek, A., Chakraborty, T., Kanellopoulou, C., Jensen, K., Cobb, B.S., Merkenschlager, M., Rajewsky, N., and Rajewsky, K. (2008). Dicer ablation affects antibody diversity and cell survival in the B lymphocyte lineage. Cell *132*, 860–874. https://doi.org/10.1016/j.cell.2008.02.020.

Lepko, T., Pusch, M., Müller, T., Schulte, D., Ehses, J., Kiebler, M., Hasler, J., Huttner, H.B., Vandenbroucke, R.E., Vandendriessche, C., et al. (2019). Choroid plexus-derived miR-204 regulates the number of quiescent neural stem cells in the adult brain. EMBO J. *38*, e100481. https://doi.org/10.15252/embj.2018100481.

Liu, C., Teng, Z.Q., Santistevan, N.J., Szulwach, K.E., Guo, W., Jin, P., and Zhao, X. (2010). Epigenetic regulation of miR-184 by MBD1 governs neural stem cell proliferation and differentiation. Cell Stem Cell *6*, 433–444. https://doi.org/10.1016/j.stem.2010.02.017.

Liu, X.S., Chopp, M., Wang, X.L., Zhang, L., Hozeska-Solgot, A., Tang, T., Kassis, H., Zhang, R.L., Chen, C., Xu, J., and Zhang, Z.G. (2013). MicroRNA-17-92 cluster mediates the proliferation and survival of neural progenitor cells after stroke. J. Biol. Chem. *288*, 12478–12488. https://doi.org/10.1074/jbc.M112.449025.

Livak, K.J., and Schmittgen, T.D. (2001). Analysis of relative gene expression data using real-time quantitative PCR and the 2(-Delta Delta C(T)) Method. Methods *25*, 402–408. https://doi.org/10.1006/meth.2001.1262.

Llorens-Bobadilla, E., Zhao, S., Baser, A., Saiz-Castro, G., Zwadlo, K., and Martin-Villalba, A. (2015). Single-cell transcriptomics reveals a population of dormant neural stem cells that become activated upon brain injury. Cell Stem Cell *17*, 329–340. https://doi.org/10.1016/j.stem.2015.07.002.

Mao, S., Li, H., Sun, Q., Zen, K., Zhang, C.Y., and Li, L. (2014). miR-17 regulates the proliferation and differentiation of the neural precursor cells during mouse corticogenesis. FEBS J. *281*, 1144–1158. https://doi.org/10.1111/febs.12680.

Mavrakis, K.J., Wolfe, A.L., Oricchio, E., Palomero, T., de Keersmaecker, K., McJunkin, K., Zuber, J., James, T., Khan, A.A., Leslie, C.S., et al. (2010). Genome-wide RNA-mediated interference screen identifies miR-19 targets in Notch-induced T-cell acute lymphoblastic leukaemia. Nat. Cell Biol. *12*, 372–379. https://doi.org/10.1038/ncb2037.

Menn, B., Garcia-Verdugo, J.M., Yaschine, C., Gonzalez-Perez, O., Rowitch, D., and Alvarez-Buylla, A. (2006). Origin of oligodendrocytes in the subventricular zone of the adult brain. J. Neurosci. *26*, 7907–7918. https://doi.org/10.1523/JNEUROSCI.1299-06.2006.

Mestdagh, P., Hartmann, N., Baeriswyl, L., Andreasen, D., Bernard, N., Chen, C., Cheo, D., D'Andrade, P., DeMayo, M., Dennis, L., et al. (2014). Evaluation of quantitative miRNA expression platforms in the microRNA quality control (miRQC) study. Nat. Methods *11*, 809–815. https://doi.org/10.1038/nmeth.3014.

Mi, S., Li, Z., Chen, P., He, C., Cao, D., Elkahloun, A., Lu, J., Pelloso, L.A., Wunderlich, M., Huang, H., et al. (2010). Aberrant overexpression and function of the miR-17-92 cluster in MLL-rearranged acute leukemia. Proc. Natl. Acad. Sci. USA *107*, 3710–3715. https://doi.org/10.1073/pnas.0914900107.

Mirzadeh, Z., Doetsch, F., Sawamoto, K., Wichterle, H., and Alvarez-Buylla, A. (2010). The subventricular zone en-face: wholemount staining and ependymal flow. J. Vis. Exp., e1938. https://doi.org/10.3791/1938.

Mirzadeh, Z., Merkle, F.T., Soriano-Navarro, M., Garcia-Verdugo, J.M., and Alvarez-Buylla, A. (2008). Neural stem cells confer unique pinwheel architecture to the ventricular surface in neurogenic regions of the adult brain. Cell Stem Cell *3*, 265–278. https://doi.org/10.1016/j.stem.2008.07.004.

Mu, P., Han, Y.C., Betel, D., Yao, E., Squatrito, M., Ogrodowski, P., de Stanchina, E., D'Andrea, A., Sander, C., and Ventura, A. (2009). Genetic dissection of the miR-17∼92 cluster of microRNAs in Myc-induced B-cell lymphomas. Genes Dev. *23*, 2806–2811. https://doi.org/10.1101/gad.1872909.

Nait-Oumesmar, B., Decker, L., Lachapelle, F., Avellana-Adalid, V., Bachelin, C., and Baron-Van Evercooren, A. (1999). Progenitor cells of the adult mouse subventricular zone proliferate, migrate and differentiate into oligodendrocytes after demyelination. Eur. J. Neurosci. *11*, 4357–4366. https://doi.org/10.1046/j.1460-9568.1999.00873.x.

Naka-Kaneda, H., Nakamura, S., Igarashi, M., Aoi, H., Kanki, H., Tsuyama, J., Tsutsumi, S., Aburatani, H., Shimazaki, T., and Okano, H. (2014). The miR-17/106-p38 axis is a key regulator of the neurogenic-to-gliogenic transition in developing neural stem/progenitor cells. Proc. Natl. Acad. Sci. USA *111*, 1604–1609. https://doi.org/10.1073/pnas.1315567111.

O'Brien, J., Hayder, H., Zayed, Y., and Peng, C. (2018). Overview of MicroRNA biogenesis, mechanisms of actions, and circulation. Front. Endocrinol. *9*, 402. https://doi.org/10.3389/fendo.2018.00402.

Obernier, K., and Alvarez-Buylla, A. (2019). Neural stem cells: origin, heterogeneity and regulation in the adult mammalian brain. Development *146*, dev156059. https://doi.org/10.1242/dev.156059.

Olive, V., Bennett, M.J., Walker, J.C., Ma, C., Jiang, I., Cordon-Cardo, C., Li, Q.J., Lowe, S.W., Hannon, G.J., and He, L. (2009). miR-19 is a key oncogenic

component of mir-17-92. Genes Dev. *23*, 2839–2849. https://doi.org/10.1101/gad.1861409.

Olive, V., Jiang, I., and He, L. (2010). mir-17-92, a cluster of miRNAs in the midst of the cancer network. Int. J. Biochem. Cell Biol. *42*, 1348–1354. https://doi.org/10.1016/j.biocel.2010.03.004.

Ortega, F., Gascón, S., Masserdotti, G., Deshpande, A., Simon, C., Fischer, J., Dimou, L., Chichung Lie, D., Schroeder, T., and Berninger, B. (2013). Oligodendrogliogenic and neurogenic adult subependymal zone neural stem cells constitute distinct lineages and exhibit differential responsiveness to Wnt signalling. Nat. Cell Biol. *15*, 602–613. https://doi.org/10.1038/ncb2736.

Ota, A., Tagawa, H., Karnan, S., Tsuzuki, S., Karpas, A., Kira, S., Yoshida, Y., and Seto, M. (2004). Identification and characterization of a novel gene, C13orf25, as a target for 13q31-q32 amplification in malignant lymphoma. Cancer Res. *64*, 3087–3095. https://doi.org/10.1158/0008-5472.can-03-3773.

Pastrana, E., Cheng, L.C., and Doetsch, F. (2009). Simultaneous prospective purification of adult subventricular zone neural stem cells and their progeny. Proc. Natl. Acad. Sci. USA *106*, 6387–6392. https://doi.org/10.1073/pnas.0810407106.

Pathania, M., Torres-Reveron, J., Yan, L., Kimura, T., Lin, T.V., Gordon, V., Teng, Z.Q., Zhao, X., Fulga, T.A., Van Vactor, D., and Bordey, A. (2012). miR-132 enhances dendritic morphogenesis, spine density, synaptic integration, and survival of newborn olfactory bulb neurons. PLoS One *7*, e38174. https://doi.org/10.1371/journal.pone.0038174.

Paul, A., Chaker, Z., and Doetsch, F. (2017). Hypothalamic regulation of regionally distinct adult neural stem cells and neurogenesis. Science *356*, 1383–1386. https://doi.org/10.1126/science.aal3839.

Petryniak, M.A., Potter, G.B., Rowitch, D.H., and Rubenstein, J.L.R. (2007). Dlx1 and Dlx2 control neuronal versus oligodendroglial cell fate acquisition in the developing forebrain. Neuron *55*, 417–433. https://doi.org/10.1016/j.neuron.2007.06.036.

Ponti, G., Obernier, K., Guinto, C., Jose, L., Bonfanti, L., and Alvarez-Buylla, A. (2013). Cell cycle and lineage progression of neural progenitors in the ventricular-subventricular zones of adult mice. Proc. Natl. Acad. Sci. USA *110*, E1045–E1054. https://doi.org/10.1073/pnas.1219563110.

Shen, Q., Wang, Y., Kokovay, E., Lin, G., Chuang, S.M., Goderie, S.K., Roysam, B., and Temple, S. (2008). Adult SVZ stem cells lie in a vascular niche: a quantitative analysis of niche cell-cell interactions. Cell Stem Cell *3*, 289–300. https://doi.org/10.1016/j.stem.2008.07.026.

Sohn, J., Orosco, L., Guo, F., Chung, S.H., Bannerman, P., Mills Ko, E., Zarbalis, K., Deng, W., and Pleasure, D. (2015). The subventricular zone continues to generate corpus callosum and rostral migratory stream astroglia in normal adult mice. J. Neurosci. *35*, 3756–3763. https://doi.org/10.1523/JNEUROSCI.3454-14.2015.

Stringer, C., Wang, T., Michaelos, M., and Pachitariu, M. (2021). Cellpose: a generalist algorithm for cellular segmentation. Nat. Methods *18*, 100–106. https://doi.org/10.1038/s41592-020-01018-x.

Szulwach, K.E., Li, X., Smrt, R.D., Li, Y., Luo, Y., Lin, L., Santistevan, N.J., Li, W., Zhao, X., and Jin, P. (2010). Cross talk between microRNA and epigenetic regulation in adult neurogenesis. J. Cell Biol. *189*, 127–141. https://doi.org/10.1083/jcb.200908151.

Tung, Y.T., Lu, Y.L., Peng, K.C., Yen, Y.P., Chang, M., Li, J., Jung, H., Thams, S., Huang, Y.P., Hung, J.H., and Chen, J.A. (2015). Mir-17 approximately 92 governs motor neuron subtype survival by mediating nuclear PTEN. Cell Rep. *11*, 1305–1318. https://doi.org/10.1016/j.celrep.2015.04.050.

Ventura, A., Young, A.G., Winslow, M.M., Lintault, L., Meissner, A., Erkeland, S.J., Newman, J., Bronson, R.T., Crowley, D., Stone, J.R., et al. (2008). Targeted deletion reveals essential and overlapping functions of the miR-17 through 92 family of miRNA clusters. Cell *132*, 875–886. https://doi.org/10.1016/j.cell.2008.02.019.

Xiao, C., Srinivasan, L., Calado, D.P., Patterson, H.C., Zhang, B., Wang, J., Henderson, J.M., Kutok, J.L., and Rajewsky, K. (2008). Lymphoproliferative disease and autoimmunity in mice with increased miR-17-92 expression in lymphocytes. Nat. Immunol. *9*, 405–414. https://doi.org/10.1038/ni1575.

Xu, S., Ou, X., Huo, J., Lim, K., Huang, Y., Chee, S., and Lam, K.P. (2015). Mir-17-92 regulates bone marrow homing of plasma cells and production of immunoglobulin G2c. Nat. Commun. *6*, 6764. https://doi.org/10.1038/ncomms7764.

Yuzwa, S.A., Borrett, M.J., Innes, B.T., Voronova, A., Ketela, T., Kaplan, D.R., Bader, G.D., and Miller, F.D. (2017). Developmental emergence of adult neural stem cells as revealed by single-cell transcriptional profiling. Cell Rep. *21*, 3970–3986. https://doi.org/10.1016/j.celrep.2017.12.017.

Zhang, L., Zhang, S., Yao, J., Lowery, F.J., Zhang, Q., Huang, W.C., Li, P., Li, M., Wang, X., Zhang, C., et al. (2015). Microenvironment-induced PTEN loss by exosomal microRNA primes brain metastasis outgrowth. Nature *527*, 100–104. https://doi.org/10.1038/nature15376.

Zhao, C., Sun, G., Li, S., Lang, M.F., Yang, S., Li, W., and Shi, Y. (2010). MicroRNA let-7b regulates neural stem cell proliferation and differentiation by targeting nuclear receptor TLX signaling. Proc. Natl. Acad. Sci. USA *107*, 1876–1881. https://doi.org/10.1073/pnas.0908750107.

Zhao, C., Sun, G., Li, S., and Shi, Y. (2009). A feedback regulatory loop involving microRNA-9 and nuclear receptor TLX in neural stem cell fate determination. Nat. Struct. Mol. Biol. *16*, 365–371. https://doi.org/10.1038/nsmb.1576.

STAR★METHODS

KEY RESOURCES TABLE

REAGENT or RESOURCE	SOURCE	IDENTIFIER
Antibodies		
Rabbit polyclonal anti-β-Catenin (1:200)	Cell Signaling	Cat# 9587, RRID: AB_10695312
Rabbit polyclonal anti-cleaved caspase 3 (1:100)	Cell Signaling	Cat# 9661 RRID: AB_2341188
Rat monoclonal PE-conjugated anti-mCD24 (1:500)	BD Biosciences	Cat# 553262; RRID:AB_394741
Rat monoclonal anti-CD24, FITC Conjugated, Clone M1/69 (1:1000)	BD Biosciences	Cat# 553261; RRID:AB_394740
Rat monoclonal Alexa Fluor 700 anti-mouse CD24 (1:150)	BioLegend	Cat# 101836; RRID:AB_2566730
Rat monoclonal biotinylated anti-mCD133 (1:300)	Thermo Fisher Scientific	Cat# 13-1331-82; RRID:AB_466591
Sheep Anti-Digoxigenin, AP Conjugated	Roche	Cat# 11093274910; RRID:AB_514497
Mouse polyclonal anti-DLX2 (1:50)	Santa Cruz	Cat# sc-18140; RRID:AB_2292994
Goat polyclonal anti-doublecortin (DCX) (1:100)	Santa Cruz	Cat# sc-8066; RRID: AB_2088494
Guinea pig monoclonal anti-DCX (1:1000)	Millipore	Cat# AB5910; RRID:AB_2230227
Rabbit polyclonal anti-DsRed (1:500)	Clontech	Cat# 632496; RRID: AB_10013483
Goat polyclonal anti-EGFR (1:100)	R&D	Cat# AF1280; RRID: AB_354717
Rabbit monoclonal anti-EGFR (1:100)	abcam	Cat# 52894; RRID: AB_869579
Rat monoclonal anti-GFAP (1:1000)	Invitrogen	Cat# 13-0300; RRID:AB_2532994
Chicken polyclonal anti-GFAP (1:600)	Millipore	Cat# PA1-10004; RRID: AB_1074620
Rabbit polyclonal anti-Glutamine synthetase (1:100)	Abcam	Cat# ab73593; RRID: AB_2247588
Rabbit polyclonal anti-Ki67 (1:100)	Abcam	Cat# ab15580; RRID: AB_443209
Rat monoclonal anti-Ki67 (1:200)	Thermo Fisher	Cat# 14-5698-80; RRID:AB_10853185
Rabbit monoclonal anti-MCM2 (1:1000)	Cell signaling	Cat# 3619; RRID: AB_2142137
Rabbit polyclonal anti-NG2 (1:100)	Millipore	Cat# AB5320; RRID: AB_91789;
Mouse monoclonal anti-O4 (1:150)	R&D	Cat# MAB1326, RRID:AB_357617
Rabbit polyclonal anti-OLIG2 (1:100)	Millipore	Cat# AB9610; RRID: AB_570666
Goat polyclonal anti-OLIG2 (1:100)	R&D	Cat# AF2418; RRID:AB_2157554
Goat polyclonal anti-PDGFRα (1:150)	R&D	Cat# AF1062; RRID: AB_2236897
Mouse monoclonal anti-TUJ1 (1:250)	Covance	Cat# MMS-435P; RRID:AB_2313773
Chemicals, peptides, and recombinant proteins		
(−)-Tetramisole hydrochloride	Sigma	Cat# L9756
(Z)-4-Hydroxytamoxifen	Sigma	Cat# H7904
Acetic anhydride	Sigma	Cat# 320102
Annexin V-Alexa647	Invitrogen/Life technologies	Cat# A23204
Antibiotic/Antimycotic	Gibco	Cat# 15240-062
Apo-transferrin	Sigma	Cat# T2252
Aqua Polymount	Brunschwig	Cat# 18606-20
B-27 supplement	Invitrogen/Life technologies	Cat# 17504044
bFGF Recombinant Human Protein	Invitrogen/Life technologies	Cat# 13256-029
Blocking solution	Roche	Cat# 11096176001
BSA	Sigma	Cat# A7030
Corn oil	Sigma	Cat# C8267

(*Continued on next page*)

Continued

REAGENT or RESOURCE	SOURCE	IDENTIFIER
DAPI	Invitrogen/Life technologies	Cat# D1306
Denhardt's Solution 50x	Sigma	Cat# D2532
Deoxyribonucleic acid, single stranded from salmon testes	Sigma	Cat# D7656
Diethyl pyrocarbonate (DEPC)	Sigma	Cat# 159220
DMEM/F12	Invitrogen/Life technologies	Cat# 21331046
DNase I	Worthington	Cat# LS002139
EDTA	Sigma	Cat# EDS
EGF-Alexa647 (1:300)	Invitrogen/Life technologies	Cat# E-35351
Epidermal Growth Factor (EGF), Murine, Natural	ThermoFisher scientific	Cat# 53003-018
Fetal bovine serum	Gibco	Cat# 301146
Fibronectin	Sigma	Cat# F2006
FluorSave	Millipore	Cat# 345789
Formamide	Sigma	Cat# 47670
Glucose	Sigma	Cat# G-7021
HBSS	Invitrogen/Life technologies	Cat# 14175-103
HCl	Sigma	Cat# 84415
Heparin sodium salt	Sigma	Cat# H3149
Insulin from bovine pancreas	Sigma	Cat# I6634
Insulin-Selenium-Transferrin	Invitrogen/Life technologies	Cat# 51500-056
Maleic acid	Sigma	Cat# M0375
Matrigel growth factor reduced	BD	Cat# 354230
N-2	Invitrogen/Life technologies	Cat# 17502048
NBT/BCIP Stock solution	Roche	Cat# 11681451001
Normal Donkey Serum	Lucerna chem	Cat# GTX73245
Ovomucoid	Worthington	Cat# LS003087
Papain	Worthington	Cat# LS003119
Paraformaldehyde (PFA)	Electron Microscopy sciences	Cat# 15714
PBS (10X)	Invitrogen/Life technologies	Cat# 70011-051
Percoll	Sigma	Cat# P1644
Phenol red	Sigma	Cat# P0290
PIPES	Sigma	Cat# P1851
Poly-D-Lysine	Sigma	Cat# P1024
Progesterone	Sigma	Cat# P6149
Proteinase K	Thermo Fisher	Cat# EO0492
Putrescine	Sigma	Cat# P5780
Sheep serum	Sigma	Cat# S2263
Sodium bicarbonate	Sigma	Cat# S8761
Sodium selenite	Sigma	Cat# S9133
SSC buffer (20X)	Sigma	Cat# S6639
Streptavidin PE-Cy7 (1:500)	Thermo Fisher Scientific	Cat# 25-4317-82; RRID:AB_10116480
Superfrost™ Plus Microscope Slides	Fisher Scientific	Cat# 12-550-15
Tamoxifen	Sigma	Cat# 85256
Triethanolamine	Sigma	Cat# 90279
Triton X-100	Sigma	Cat# T8787
Tween 20	Sigma	Cat# P9416

(*Continued on next page*)

Continued

REAGENT or RESOURCE	SOURCE	IDENTIFIER
Critical commercial assays		
TaqMan® Array Rodent MicroRNA A Cards v2.0	Applied Biosystem	Cat# 4398967
miRCURY LNA SYBR Green PCR Kit	Qiagen	Cat# 339346
miRCURY LNA RT Kit	Qiagen	Cat# 339340
Lipofectamine 3000	Thermo Fisher Scientific	Cat# L3000008
Dual-Luciferase Reporter Assay System	Promega	Cat# E1910
Prom-II^{TM} Reverse Transcriptase	Promega	Cat# A3800
KAPA SYBR® FAST	Merck	Cat# SFUKB
Experimental models: Organisms/strains		
Mouse: hGFAP::GFP	The Jackson Laboratory	JAX: 003257
Mouse: CD1	Charles River	022
Mouse: RjOrl:SWISS	Janvier Labs	RjOrl:SWISS
Mouse: Mirc1$^{tm1.1Tyj}$/J	The Jackson Laboratory	JAX: 008458
Mouse: B6.Cg-Tg(GFAP-cre/ERT2) 505Fmv/J	The Jackson Laboratory	JAX: 012849
Mouse: B6.Cg-Gt(ROSA) 26Sor$^{tm14(CAG-tdTomato)Hze}$	The Jackson Laboratory	JAX: 007914
Mouse: Gt(ROSA)26 Sor$^{tm4(ACTB-tdTomato,-EGFP)Luo}$/J	The Jackson Laboratory	JAX: 007576
Mouse: CAGG::CreER^{T2}; miR-17∼92$^{fl/fl}$	Wichterle laboratory, Columbia University	N/A
Mouse: CAGG::CreER$^{T2+/-}$ or $^{-/-}$; miR-17∼92$^{fl/fl}$; ROSA$^{(ACTB-tdTomato,-EGFP)}$	This study	N/A
Mouse: hGFAP::CreER^{T2}; miR-17∼92$^{+/+}$ or $^{fl/fl}$; Ai14	This study	N/A
Oligonucleotides		
miR-16-5p miRCURY LNA miRNA PCR Assay	Qiagen	Cat# YP00205702
miR-17-5p miRCURY LNA miRNA PCR Assay	Qiagen	Cat# YP02119304
miR-17-3p miRCURY LNA miRNA PCR Assay	Qiagen	Cat# YP00205325
miR-18a-5p miRCURY LNA miRNA PCR Assay	Qiagen	Cat# YP00204207
miR-19a-3p miRCURY LNA miRNA PCR Assay	Qiagen	Cat# YP00205862
miR-19b-3p miRCURY LNA miRNA PCR Assay	Qiagen	Cat# YP00204450
miR-20a-5p miRCURY LNA miRNA PCR Assay	Qiagen	Cat# YP00204292
miR-92a-3p miRCURY LNA miRNA PCR Assay	Qiagen	Cat# YP00205947
Scramble-miR miRCURY LNA Detection probe, negative control	Qiagen	Cat# YD00699004
mmu-miR-17-5p miRCURY LNA miRNA Detection Probe (1 nmol)	Qiagen	Cat# YD00615470
mmu-miR-18a-5p miRCURY LNA miRNA Detection Probe (1 nmol)	Qiagen	Cat# YD00616983
mmu-miR-19a-3p miRCURY LNA miRNA Detection Probe (1 nmol)	Qiagen	Cat# YD00615459
mmu-miR-19b-3p miRCURY LNA miRNA Detection Probe (1 nmol)	Qiagen	Cat# YD00619863

(*Continued on next page*)

Continued

REAGENT or RESOURCE	SOURCE	IDENTIFIER
mmu-miR-20a-5p miRCURY LNA miRNA Detection Probe (1 nmol)	Qiagen	Cat# YD00616215
mmu-miR-92a-3p miRCURY LNA miRNA Detection Probe (1 nmol)	Qiagen	Cat# YD00615578
Deposited data		
miRNA profiling data of V-SVZ populations	This study	GEO: GSE217425
RNAseq data of V-SVZ populations	Delgado et al. (2021)	GEO: GSE118009
Software and algorithms		
Rstudio	https://www.rstudio.com	RRID:SCR_000432
Fiji	https://imagej.net/software/fiji	RRID:SCR_002285
MetaCore	Thompson Reuters, NY	RRID:SCR_008125
ExpressionSuite software v1.3	Thermo Fisher	RRID:SCR_021095
R-commander	https://cran.r-project.org/web/packages/Rcmdr	RRID:SCR_001905

RESOURCE AVAILABILITY

Lead contact

Further information and requests for resources and reagents should be directed to and will be fulfilled by the Lead Contact, Fiona Doetsch (fiona.doetsch@unibas.ch).

Materials availability

All unique/stable reagents generated in this study are available from the lead contact without restriction.

Data and code availability

- miRNA profiling data of V-SVZ populations have been deposited at GEO and are publicly available as of the date of publication. Accession numbers are listed in the key resources table. For miR-17∼92 target analysis, this paper analyzes existing, publicly available RNA-seq data of FACS-purified populations. The accession number for these datasets are listed in the key resources table.
- This paper does not report original code.
- Any additional information required to reanalyze the data reported in this paper is available from the lead contact upon request.

EXPERIMENTAL MODEL AND SUBJECT DETAILS

Mice

All experiments were performed in accordance with institutional and national guidelines for animal use and approved by IACUC at Columbia University and the cantonal veterinary office of Basel-Stadt. All mice (males and females) were group-housed conventionally with *ad libitum* food and water in 12-h light/12-h dark cycles, and sacrificed at the same time of day. All mice used were two to four months old and were randomly assigned to experimental groups. The following mouse lines were used: hGFAP::GFP (The Jackson Laboratory, JAX: 003257), CD1(Charles River, 022), RjOrl:SWISS (Janvier Labs), CAGG::CreER^{T2}; miR-17∼92$^{fl/fl}$ mice (kindly provided by the Wichterle laboratory at Columbia University), Gt(ROSA)26Sor$^{tm4(ACTB-tdTomato,-EGFP)Luo}$/J mice (ROSA$^{(ACTB-tdTomato,-EGFP)}$, The Jackson Laboratory, JAX: 007576), *Mirc1*$^{tm1.1Tyj}$/J mice (The Jackson Laboratory, JAX: 008458, kindly provided by the Jeker laboratory at the University of Basel), B6.Cg-Tg(GFAP-cre/ERT2)505Fmv/J mice (hGFAP::CreER^{T2}, The Jackson Laboratory, JAX: 012849) and Gt(ROSA)26Sor$^{tm14(CAG-tdTomato)Hze}$ (Ai14; The Jackson Laboratory, JAX: 007914). We bred CAGG::CreER^{T2}; miR-17∼92$^{fl/fl}$ mice to ROSA $^{(ACTB-tdTomato,-EGFP)}$ mice to generate CAGG::CreER$^{T2+/-}$ or $^{-/-}$; miR-17∼92$^{fl/fl}$; ROSA$^{(ACTB-tdTomato,-EGFP)}$ mice [CAGG-miR-17∼92$^{fl/fl}$]. We crossed *Mirc1*$^{tm1.1Tyj}$/J mice to hGFAP::CreER^{T2} mice and Gt(ROSA)26Sor$^{tm14(CAG-tdTomato)Hze}$ mice to generate hGFAP::CreER^{T2}; miR-17∼92$^{+/+}$ or $^{fl/fl}$; Ai14 mice [miR-17∼92$^{+/+}$ and miR-17∼92$^{fl/fl}$].

METHOD DETAILS

FACS-purification strategy

The V-SVZs were dissected from heterozygous hGFAP::GFP mice (Jackson Labs) or wildtype CD-1 mice (Charles River), digested with papain (Worthington, 1,200 units per 5 mice, 10 min at 37°C) in PIPES solution [120 mM NaCl, 5 mM KCl, 50 mM PIPES (Sigma),

0.6% glucose, 1X Antibiotic/Antimycotic (Gibco), and phenol red (Sigma) in water, pH adjusted to 7.6] and mechanically dissociated to single cells after adding ovomucoid (Worthington, 0.7 mg per 5 mice) and DNAse (Worthington, 1,000 units per 5 mice). Cells were centrifuged for 10 min at 4°C without brake in 22% Percoll (Sigma) to remove myelin. Cell stainings were done in 3 steps: First, cells were incubated for 20 min with PE-conjugated anti-mCD24 (rat monoclonal, 1:500, BD Biosciences, Cat# 553262, RRID:AB_394741) and biotinylated anti-mCD133 (rat monoclonal, 1:300, clone 13A4, Thermo Fisher Scientific, Cat# 13-1331-82, RRID:AB_466591). Cells were washed by centrifugation at 1300rpm for 5min. Next, cells were incubated for 10 min with Streptavidin PE-Cy7 (1:500; Thermo Fisher Scientific, Cat# 25-4317-82, RRID:AB_10116480), and washed by centrifugation. Finally, cells were incubated with A647-complexed EGF (1:300; Molecular Probes, Cat# E-35351) for 15 min, and washed by centrifugation. All stainings and washes were carried out on ice in 1% BSA, 0.1% Glucose HBSS solution. To assess cell viability, 4′,6-diamidino-2-phenylindole (DAPI; 1:1000; Sigma) was added to the cell suspension. All cell populations were isolated in a single sort using a Becton Dickinson FACS Aria II using 13 psi pressure and 100-μm nozzle aperture and were collected in Neurosphere medium (NSM) [DMEM/F12 (Life Technologies) supplemented with 0.6% Glucose (Sigma), 1X Hepes (Life Technologies), 1X Insulin-Selenium-Transferrin (Life Technologies), N-2 (Life Technologies), and B-27 supplement (Life Technologies)]. Gates were set manually using single-color control samples and FMO controls.

miRNA profiling and qPCR analysis

For miRNA profiling, total RNA, including small RNAs, was extracted from FACS-purified populations of qNSCs (hGFAP::GFP$^+$, CD133$^+$, EGFR$^-$, CD24$^-$) (n = 3 biological replicates), aNSCs (hGFAP::GFP$^+$, CD133$^+$, EGFR$^+$, CD24$^-$) (n = 3 biological replicates) and TACs (hGFAP::GFP$^-$, CD133$^-$, EGFR$^+$, CD24$^-$) (n = 2 biological replicates) using the miRNeasy kit (Qiagen). miRNAs were pre-amplified and profiled using TaqMan® Array Rodent MicroRNA A Cards v2.0 A as specified by the manufacturer at the Genome Technology Center of New York University Langone Medical Center. Raw data was loaded into the ExpressionSuite program v1.3 (ThermoFischer) and four control RNAs (U6, sno135, sno202 and miR-16-5p) were used to normalize the dataset.

For qPCR analysis of miRNA expression, miRNA-enriched fractions were extracted from FACS-purified qNSCs, aNSCs and TACs using the miRNeasy kit (Qiagen). cDNA was synthesized using the Exiqon miRCURY LNA Universal RT microRNA kit (Qiagen). qPCR for individual miR-17∼92 members was performed using miRCURY LNA probes and miRCURY LNA SYBR Green PCR Kit (Qiagen).

In vitro assays

To isolate cells for *in vitro* assays, mixed cohorts of male and female CAGG::CreERT2$^{+/-}$ or $^{-/-}$; miR-17∼92$^{fl/fl}$; ROSA$^{(ACTB\text{-}tdTomato,\text{-}EGFP)}$ mice were processed for FACS as described above and stained with CD24-FITC (rat monoclonal, 1:1000; Cat# 553261; RRID:AB_394740), EGF-Alexa647 (1:300; Molecular Probes, Cat# E-35351), and biotinylated anti-mCD133 (rat monoclonal, 1:300, clone 13A4, Thermo Fisher Scientific, Cat# 13-1331-82; RRID:AB_466591), which was followed by secondary staining with PE-Cy7-conjugated streptavidin (1:1000; Thermo Fisher Scientific, Cat# 25-4317-82; RRID:AB_10116480). CD133$^+$ EGFR$^+$ CD24$^-$ cells were FACS-purified to obtain aNSCs and used for the following assays.

To validate deletion of the miR-17∼92 cluster *in vitro*, FACS-purified aNSCs were cultured in NSM + EGF for five days, then the medium was replaced with NSM + EGF + 250nM 4OHT for two days to induce recombination. Medium was then switched to NSM + EGF for 5 additional days to allow recombined cells to further expand. Cells were collected for sorting by trypsinization for 5 min at 37°C, followed by dissociation to single cells by pipetting and passed through a 40-μm filter. DAPI was added prior to FACS to detect dead cells. Cells were gated based on expression of tdTomato (non-recombined cells) and eGFP (recombined cells) and genomic DNA isolated for PCR. Deletion of the miR-17∼92 locus was verified using the following primers: 17∼92 deletion_F: 5′-TCGAGTATCTGACAATGTGG-3′; 17∼92 deletion_R: 5′-TAGCCAGAAGTTCCAAATTGG-3′. A band of ∼2kb indicates an intact locus, whereas a band of ∼1kb indicates deletion of miR-17∼92.

For single cell adherent assays, one FACS-purified aNSC per well was manually plated into 96 well plates previously coated with Poly-D-Lysine (Sigma, 10 μg/mL) and Fibronectin (Sigma, 2 μg/mL). During the first 24 h after plating, cells were treated with NSM + EGF, NSM + EGF +250nM 4OHT, or NSM + EGF + vehicle alone (EtOH). At 24 h, the entire media was replaced with NSM & EGF to prevent toxicity. Cells were fixed with 4% paraformaldehyde (PFA) in 0.1M phosphate buffer (PB) at 13 days post-plating and stained with DAPI (Sigma). Finally, the total number of DAPI$^+$ cells per well was quantified blind to condition.

For survival assays, during the first 24 h after plating, FACS-purified aNSCs were treated with NSM + EGF +250nM 4OHT. At 24 h the media was replaced with NSM alone for 5 days. Cells were stained with Annexin V-Alexa647 (1:500, Life Technologies), fixed for 30 min with 3.2% PFA, and stained for DAPI (1:1000, Sigma). The wells were imaged on the ZEISS Observer 7.1 at 5X. DAPI$^+$ cells were quantified for co-expression with Tomato, eGFP, and Annexin V using the cell counter plugin in FIJI. To assess survival independent of proliferation, each colony was considered as one unit.

For the neurosphere assay, FACS-purified aNSCs were plated at a density of 100 cells per well in 96-well low-attachment plates (Costar). Cells were grown in Neurosphere medium (NSM, see above) in the presence of 20 ng/mL EGF (Upstate). For the first 24 h immediately after plating, cells were also treated with 500nM hydroxytamoxifen (4OHT, Sigma) or vehicle alone (ethanol, EtOH). At 24 h, half of the media was replaced with NSM + EGF to reduce toxicity. The cells were then monitored every 2 days for neurosphere formation and recombination.

For *in vitro* differentiation, neurosphere cultures were established from miR-17–92$^{+/+}$ and miR-17∼92$^{fl/fl}$ mice as described in (Belenguer et al., 2016). Passage four neurospheres were dissociated and plated at a density of 5000 cells per well in Matrigel (BD)

precoated Nunc™ Lab-Tek™ Chamber Slide System (16 well glass slide) in control medium [DMEM/F12 (Life Technologies) supplemented with 0.6% Glucose (Sigma), 0.1% Sodium Bicarbonate (Sigma), 5mM HEPES (Gibco), 1X L-Glutamine (Sigma), 1X Antibiotic/Antimycotic (Gibco), 4mg/mL BSA (Sigma), 0.8 mg/mL Apo-transferrin (Sigma), 500 nM Bovine Insulin (Sigma), 0.2 nM Progesterone (Sigma), 0.1 mg/mL Putrescine (Sigma), 0.3 μM Sodium Selenite (Sigma)] supplemented with 0.7 U/ml Heparin sodium salt (Sigma), 20 ng/ml EGF (Thermo Fisher Scientific) and 10 ng/ml bFGF (Invitrogen). Two days later, cells were exposed to 2μM 4-hydroxytamoxifen (Sigma) for 48 h to induce recombination. Cells were then differentiated as described in (Belenguer et al., 2016). Briefly, cells were cultured for 2 days in control medium with bFGF and Heparin sodium salt (no EGF). Medium was then replaced with fresh control medium supplemented with 2% heat inactivated fetal bovine serum (FBS, Gibco) for 5 days. Cells were fixed with 4% PFA in 0.1M PB, immunostained and counterstained for DAPI. The wells were imaged on the ZEISS LSM880 at 10X. Quantification of total $DAPI^+$ nuclei and identification of TOM^+ cells were performed automatically in FIJI using a FIJI wrapper (https://github.com/BIOP/ijl-utilities-wrappers) as follows: First, nuclei were segmented using Cellpose's default model (Stringer et al., 2021) and individual nuclei were defined as independent region of interest (ROI). Next, signal intensities for TOM were measured in each ROI in order to classify and automatically count TOM^+ and TOM^- nuclei. Quantification of total $TUJ1^+$ and $O4^+$ cells and assessment of their colabeling for TOM were then performed manually using the cell counter plugin in FIJI.

Tamoxifen injections

Cre-mediated recombination in $CreER^{T2}$ transgenic mice was induced by administration of Tamoxifen (Sigma) dissolved at 30 mg/mL in 90% corn oil with 10% ethanol (Sigma). Mice were intraperitoneally injected at the dose of 120 mg/kg once per day for three consecutive days and sacrificed one or thirty days after the last tamoxifen injection.

Validation of miR-17∼92 deletion and targets

$Tomato^+$ $CD133^-$ $EGFR^+$ $CD24^-$ cells or $Tomato^-$ $CD133^-$ $EGFR^+$ $CD24^-$ cells (corresponding to TACs) were FACS-purified at 1dpi from mixed cohort of male and female miR-17∼$92^{fl/fl}$ mice as described above, using CD24-A700 (rat monoclonal, 1:150, BioLegend, Cat# 101836, RRID:AB_2566730) and EGF-Alexa647 (1:300, Molecular Probes, Cat# E-35351) antibodies. For validating miR-17∼92 deletion *in vivo*, RNA from sorted cells was extracted and fractionated according to size (<200nt for miRNA detection or >200nt for target gene analysis) using the Exiqon miRCURY RNA extraction kit. Expression of mature miRs was assayed by qPCR using Exiqon probes for miR-17-5p, miR-20a-5p, miR-92a-3p and miR-16-5p (for normalization). For identifying oligodendrogenesis-related miR-17∼92 targets, RNA from FACS-purified cells was retrotranscribed into cDNA using ImProm-II ™ Reverse Transcriptase (Promega). qPCR for *Pdgfrα, Gpr37, Olig2, Nrg1, Sp1, Yy1* and *Qki* was then performed using KAPA SYBR® FAST (Merck). Sequences of primers are as follows: *Pdgfrα:* F: 5′-CCTGGTGCTGTTGGTGATTG-3′, R: 5′-ATACCTCGGTTTCTGTTTCCAAAT-3′; *Gpr37*: F: 5′-ACCGGACACAATCTATGTTTTGG-3′, R: 5′-TCTTCCGAGCAGTCACTAGAG-3′; *Olig2*: F: 5′-GGCGGTGGCTTCAAGTCATC-3′, R: 5′-TCGGGCTCAGTCATCTGCTTC-3′, *Nrg1*: F: 5′-AGTGCCCAAATGAGTTTACTGG-3′, R: 5′-AGTTCCTCCGCTTCCATAAATTC-3′; *Sp1*: F: 5′-GCCGCCTTTTCTCAGACTC-3′, R: 5′-TTGGGTGACTCAATTCTGCTG-3′; *Yy1*: F: 5′-CAGTGGTTGAAGAGCAGATCAT-3′, R: 5′-AGGGAGTTTCTTGCCTGTCAT-3′; *Qki*: F: 5′-TAGCAGAGTACGGAAAGACATG-3′, R: 5′-GGGTATTCTTTTACAGGCACAT-3′; *Gapdh*: F: 5′-TGAGGCCAGTGCTGAGTATG-3′, R: 5′- CACATTGGGGGTAGGAACAC-3′" (Microsynth).

Tissue preparation

Mice were anesthetized by intraperitoneal injection of pentobarbital (Esconarkon) and were sacrificed by intracardial perfusion of 4% PFA in either 0.1M PB (for free-floating sections) or 1X phosphate buffer saline (PBS, for cryosections). Brains were extracted from the skull and post-fixed overnight. 25 μm thick free-floating coronal sections were cut using a vibratome (Leica VT1000S). For cryosections, after overnight fixation, brains were cryoprotected by sequential overnight incubation in 15% and 30% sucrose in 1X PBS, snap frozen in −70°C cold isopentane and stored for at least two days at −80°C. 12μm thick sections were cut on a cryostat (Leica CM3050S). Wholemounts were dissected as described in (Mirzadeh et al., 2010) from saline-perfused mice and post-fixed overnight in 4% PFA in PB 0.1M solution.

miRNA *in situ* hybridization

In situ hybridization for miRNA expression was performed on cryosections as described in Jin et al. (2016) using locked nucleic acid (LNA) probes. Briefly, scrambled, miR-17-5p, miR-18a-5p, miR-19a-3p and miR-92a-3p LNA probes (Qiagen) were 3′ end labeled with DIG–ddUTP. After fixation with 4% PFA, acetylation with the acetylation buffer (1.33% Triethanolamine, 0.25% Acetic anhydride, 20 mM HCl), treatment with proteinase K (10 mg/mL, Roche) and pre-hybridization (1X Saline sodium citrate (SSC) buffer, 50% Formamide, 0.1 mg/mL Salmon Sperm DNA Solution, 1X Denhart, 5 mM EDTA, pH7.5), brain sections were hybridized with DIG-labeled LNA probes at 65°C overnight. After washing with ice-cold wash buffer (1X SSC, 50% Formamide, 0.1% Tween 20) and 1X Maleic acid buffer containing Tween 20 (MABT), sections were blocked with the blocking buffer (1X MABT, 2% Blocking solution, 20% heat-inactivated sheep serum) and incubated with anti-DIG antibody (1:2000, Roche) overnight. Brain sections were washed with 1X MABT and the staining buffer (0.1 M NaCl, 50 mM MgCl2, 0.1 M Tris-HCl, pH9.5), stained with NBT/BCIP (Roche) at room temperature. Finally, sections were washed twice in 1X PBS for 10 min at room temperature (RT) and subjected to immunostaining as described below.

Immunostaining

Wholemounts and tissue sections were incubated in blocking solution [for wholemounts, PBS with 3% bovine serum albumin (BSA) and 1.5% Triton X-100; for tissue sections, PBS with 10% donkey normal serum supplemented with 0.03% Triton X-100 for antibodies against receptors or 0.3% Triton X-100 for all others] for 1 h at RT and then incubated in primary antibodies in blocking solution either for 36 h at 4°C or overnight at RT. After washing, sections were incubated with secondary antibodies for 1 h at RT. After washing, sections and wholemounts were counterstained with DAPI (Sigma). Sections were mounted on slides with either Aqua Polymount (Brunschwig) or FluorSave™ (Millipore Corporation).

Antibodies

The following primary antibodies were used: anti-β-Catenin (rabbit polyclonal, 1:200, Cell signaling, Cat# 9587, RRID: AB_10695312); anti-cleaved caspase 3 (rabbit polyclonal, 1:100, Cell Signaling, Cat# 9661, RRID: AB_2341188); anti-DLX2 (mouse polyclonal, 1:50, Santa Cruz, Cat# sc-18140, RRID:AB_2292994); anti-doublecortin, DCX (goat polyclonal, 1:100, Santa Cruz, Cat# sc-8066, RRID: AB_2088494); anti-DCX (guinea pig monoclonal, 1:1000, Millipore, Cat# AB5910, RRID:AB_2230227); anti-DsRed (rabbit polyclonal, 1:500, Clontech, Cat# 632496, RRID: AB_10013483); anti-EGFR (goat polyclonal,1:100, R&D, Cat# AF1280, RRID: AB_354717); anti-EGFR (rabbit monoclonal, 1:100, abcam, Cat# 52894, RRID: AB_869579); anti-GFAP (rat monoclonal, 1:1000, Invitrogen, Cat# 13-0300, RRID:AB_2532994); anti-GFAP (chicken polyclonal, 1:600, Millipore, Cat# PA1-10004, RRID: AB_1074620); anti-Glutamine synthetase (rabbit polyclonal, 1:100, abcam, Cat# ab73593, RRID: AB_2247588); anti-Ki67 (rabbit polyclonal, 1:100, abcam, Cat# ab15580, RRID: AB_443209); anti-Ki67 (rat monoclonal, 1:200, Thermo Fisher, Cat# 14-5698-80, RRID:AB_10853185); anti-MCM2 (rabbit monoclonal, 1:1000, Cell signaling, Cat# 3619, RRID: AB_2142137); anti-NG2 (rabbit polyclonal, 1:100, Millipore, Cat# AB5320, RRID: AB_91789); anti-O4 (mouse monoclonal, 1:150, R&D, Cat# MAB1326, RRID:AB_357617); anti-OLIG2 (rabbit polyclonal, 1:100, Millipore, Cat# AB9610, RRID: AB_570666); anti-OLIG2 (goat polyclonal, 1:150, R&D, Cat# AF2418, RRID:AB_2157554); anti-PDGFRα (goat polyclonal, 1:150, R&D, Cat# AF1062, RRID: AB_2236897), anti-TUJ1 (mouse monoclonal, 1:250, Covance, Cat# MMS-435P, RRID:AB_2313773). The following secondary antibodies were used: Alexa Fluor-conjugated (405, 1:250, abcam; 488, 647, 568, 1:600, Molecular probes), Cy3-conjugated (1:1000, Jackson ImmunoResearch).

Brain section imaging and quantification

Tile scans of the entire dorsoventral extent of the V-SVZ of at least four different rostro-caudal levels (Bregmas: ∼+1mm, ∼+0.70mm, ∼+0.3mm and ∼+0mm) were acquired on a Zeiss LSM800 or LSM880 confocal microscope at 25X or 40X with 1.5μm distance between focal planes. Immunostaining using more than 4 fluorophores was imaged on a NikonTi2 widefield microscope at 40X. TOM^+ and TOM^- cells were quantified using the Cell Counter plug-in in FIJI. For each rostro-caudal level, cell percentages of different cell populations over total TOM^+ or TOM^- cells or per specific population were calculated. Cell percentages of the same population from different rostro-caudal levels per mouse were averaged and the average values from control and deleted mice were then compared to identify statistically significant differences in cell populations. Images from wholemounts were acquired on Zeiss LSM700 or 800 confocals at 40X. For intraventricular OPCs quantification, at least 5 mice per group were analyzed. Mice with less than 15 recombined intraventricular OPCs per wholemount were excluded.

Bioinformatic analysis

A list of genes expressed in early stages of the lineage was compiled from gene expression datasets of FACS-purified V-SVZ NSC populations ($PDGFR\beta^+$ $CD133^+$, $PDGFR\beta^+$ $CD133^+$ $EGFR^+$ and $PDGFR\beta^-$ $CD133^+$ $EGFR^+$) (Delgado et al., 2021). Computationally predicted targets for the guide and star forms of individual members of the miR-17∼92 cluster (miR-17, 18a, 19a, 20a, 19b, 92a and miR-17*) were generated from the online platforms Targetscan, PicTar, microcosm and miRDB. The gene expression list and miR target list were then compared to find overlap. Finally, the resulting list of miR-17∼92 targets was analzyed using MetaCore (Thompson Reuters, New York, NY) performing enrichment analysis by pathway maps.

Plasmid constructs for luciferase assay

Fragments of the 3′UTR of *Pdgfrα* (1'791 bp) and *Qki* (1'017 bp), encompassing binding sites for members of the miR-17∼92 cluster, were amplified from mouse genomic DNA by PCR and cloned into psiCHECK™-2 vector from Promega at the XhoI/NotI restriction sites (In-Fusion HD cloning kit, Clontech Laboratories). Psi-CHECK2-hoxa5 3′UTR luciferase reporter (Tung et al., 2015) was generously provided by Jun-An Chen. To generate miR-17∼92 expression construct, the entire miR-17∼92 cluster sequence was amplified from the pKO-II-miR-17∼92 vector (Addgene) by PCR and cloned into the pSR-GFP expression vector (Cheng et al., 2009) at the HindIII/XhoI restriction sites (In-Fusion HD cloning kit, Clontech Laboratories). All constructs were sequenced (Microsynth).Sequences of primers are as follows: Pdgfrα 3′UTR: F: 5′-GTCTGTGACTTTTAAGGATGC-3′, R: 5′-CCACACCACCATGTTGGGAAC-3′; Qki 3′UTR: F: 5′-GATATTAGTCCTTTGGAGAAC-3′, R: 5′-GTGCCTTCGAACTTTAGTAG-3′; miR-17∼92: F: 5′-GCTGTAATTGATG TTTGTGAC-3′, R: 5′-ATCCCGTTTTACACACCAACG-3′ (Microsynth).

Luciferase reporter assay

HEK293 cells were plated at a density of 9 × 10^4 cells in poly-L-lysine pre-coated 48-well plates, expanded for 18h, and transfected with 62.5 ng luciferase reporter and 187.5 ng miRNA vector (1:3 ratio) using 0.5 μL of PLUS Reagent and 1 μL of Lipofectamine 3000 (Life Technology). Cells were incubated with lipofectamine-DNA complexes for 24 h prior to changing medium containing lipofectamine with fresh medium. Transfected HEK293 were grown for additional 24 h before performing luciferase assay. Finally, cells were lysed and processed for luciferase assays using the Dual-Luciferase Reporter Assay System (Promega). Luciferase activity was measured using the TECAN Spark Plate Reader. The ratio between renilla and firefly luciferase activities was calculated for all luciferase reporters. The data were then normalized to the respective miRNA empty vector conditions. All luciferase activity data are presented as means ± SD of values from three experiments, each performed in duplicates.

QUANTIFICATION AND STATISTICAL ANALYSIS

For analysis of miRNA microarray data, miRNA expression was first normalized to U6, sno202, sno135, and miR-16-5p, using the same threshold and baseline settings as in (Eriksen et al., 2016; Mestdagh et al., 2014), and differential expression between qNSCs and aNSCs determined by unpaired t test, ($p < 0.05$). Both normalization and analysis were performed in the ExpressionSuite program v1.3 (ThermoFischer). For qPCR analysis of miRNA and mRNA target expression, data were normalized to miR-16-5p or *Gapdh* respectively and analyzed by the 2-ΔΔCT method (Livak and Schmittgen, 2001). For neurospheres and the differentiation assay, differences were assessed using paired two-tailed Student's t-test using Prism 6 software. For single cell adherent cultures, two-sided Wilcoxon rank-sum test was used to assess overall changes in the distribution of the outcomes (given number of cells per well), followed by Fisher's exact test, to later identify which of the outcomes was responsible for the difference. These analyses were performed using R-commander. For *in vivo* experiments, two-way statistical comparisons were conducted by two-tailed unpaired Student's t-test of arcsine-transformed relative values (percentages) using Microsoft Excel. Finally, for pathway analysis, significance was defined by p value <0.05 and False Discovery Rate <0.05. For all comparisons, significance was established at *$p < 0.05$, **$p < 0.01$, ***$p < 0.001$, ****$p < 0.0001$, *****$p < 0.00001$. In all graphs, error bars represent standard deviation (SD).